MCB Journals.ASM.org

The Oxidation Status of Mic19 Regulates MICOS Assembly

Paulina Sakowska,[a] Daniel C. Jans,[b,c] Karthik Mohanraj,[a] Dietmar Riedel,[d] Stefan Jakobs,[b,c] Agnieszka Chacinska[a]

International Institute of Molecular and Cell Biology, Warsaw, Poland[a]; Department of NanoBiophotonics, Max Planck Institute for Biophysical Chemistry, Göttingen, Germany[b]; Department of Neurology, University Medical Center, Göttingen, Germany[c]; Electron Microscopy Facility, Max Planck Institute for Biophysical Chemistry, Göttingen, Germany[d]

The function of mitochondria depends on the proper organization of mitochondrial membranes. The morphology of the inner membrane is regulated by the recently identified mitochondrial contact site and crista organizing system (MICOS) complex. MICOS mutants exhibit alterations in crista formation, leading to mitochondrial dysfunction. However, the mechanisms that underlie MICOS regulation remain poorly understood. MIC19, a peripheral protein of the inner membrane and component of the MICOS complex, was previously reported to be required for the proper function of MICOS in maintaining the architecture of the inner membrane. Here, we show that human and *Saccharomyces cerevisiae* MIC19 proteins undergo oxidation in mitochondria and require the mitochondrial intermembrane space assembly (MIA) pathway, which couples the oxidation and import of mitochondrial intermembrane space proteins for mitochondrial localization. Detailed analyses identified yeast Mic19 in two different redox forms. The form that contains an intramolecular disulfide bond is bound to Mic60 of the MICOS complex. Mic19 oxidation is not essential for its integration into the MICOS complex but plays a role in MICOS assembly and the maintenance of the proper inner membrane morphology. These findings suggest that Mic19 is a redox-dependent regulator of MICOS function.

Mitochondria are essential organelles in eukaryotic cells and play a key role in many cellular processes, including energy conversion; the synthesis of amino acids, lipids, and heme; and apoptosis. Mitochondria are enveloped by the outer membrane (OM) and composed of two aqueous compartments: the matrix and intermembrane space (IMS), which are separated by the inner membrane (IM). The IM is further divided into the inner boundary membrane (IBM; which is adjacent to the outer membrane) and invaginations (called cristae) that protrude into the matrix. Cristae are attached to the IBM by narrow, usually tube-shaped structures called crista junctions (1, 2).

One of the mechanisms that are responsible for the mitochondrial IM architecture involves the recently discovered mitochondrial contact site and crista organizing system (MICOS) complex (previously known as MINOS/MitOS) (3–9). MICOS is an evolutionarily conserved complex that consists of six proteins in *Saccharomyces cerevisiae* and seven proteins in higher eukaryotes that have been identified to date (3–16). The deletion or knockdown of MICOS components was shown to lead to defects in mitochondrial morphology, accompanied by mitochondrial dysfunction. Deletion of subunits of the MICOS complex resulted in a partial or almost entire loss of crista junctions. In the case of Mic19, a partial reduction in the number of crista junctions was reported. In transmission electron microscopy (EM) of MICOS mutants, the mitochondria often appear to have stacked or onion-like inner membranes, depending on the orientation of the imaged section (3–7, 10, 12, 14, 17, 18).

The MICOS complex builds a wide interaction network with proteins with different mitochondrial localizations and functions. MICOS was shown to interact with translocase of the outer membrane (TOM), sorting and assembly machinery (SAM), Ugo1, porin (VDAC), and the components of the mitochondrial intermembrane space assembly (MIA) pathway (4–6, 11, 19–23). The TOM complex is the main entry gate for precursor proteins that are directed from the cytosol to mitochondria. Precursors that emerge from the TOM complex at the intermembrane space site of the outer membrane are subsequently recognized by specific translocases. These translocases transfer precursor proteins to their destined mitochondrial compartments (24–27). The import of proteins that are targeted to the intermembrane space is facilitated by the MIA pathway (28, 29). Precursors are recognized by Mia40, an oxidoreductase that binds to its substrates via a disulfide bond. Next, the disulfide bonds are transferred to the substrate, resulting in its oxidation and thus enabling proper folding and assembly into mature, functional protein complexes (27, 29–33). Classic MIA pathway substrates are small (<20-kDa) proteins that contain specific twin Cys-X_3-Cys or Cys-X_9-Cys motifs that typically form two disulfide bonds (34–37). To maintain oxidation cycles, Mia40 cooperates with the sulfhydryl oxidase Erv1 (30, 38–40). Mic60, one of the key components of the MICOS complex, was recently shown to play a role in the regulation of protein transport via the MIA pathway (6).

Mic19 and MIC19 are present in the MICOS complex in yeast and humans, respectively. Human MIC19 (CHCHD3 or MINOS3) possesses five cysteine residues, four of which are arranged in a twin Cys-X_9-Cys motif of the coiled-coil helix coiled-coil helix (CHCH) domain that is typical for MIA substrates. Previous studies (12, 41) reported that the CHCH do-

Received 12 June 2015 **Returned for modification** 29 June 2015
Accepted 4 September 2015

Accepted manuscript posted online 28 September 2015

Citation Sakowska P, Jans DC, Mohanraj K, Riedel D, Jakobs S, Chacinska A. 2015. The oxidation status of Mic19 regulates MICOS assembly. Mol Cell Biol 35:4222–4237. doi:10.1128/MCB.00578-15.

Address correspondence to Agnieszka Chacinska, achacinska@iimcb.gov.pl.

Copyright © 2015 Sakowska et al. This is an open-access article distributed under the terms of the Creative Commons Attribution-Noncommercial-ShareAlike 3.0 Unported license, which permits unrestricted noncommercial use, distribution, and reproduction in any medium, provided the original author and source are credited.

Downloaded from http://mcb.asm.org/ on January 18, 2016 by NIEDERSAECHSISCHE STAATS- UND UNIVERSITAETSBIBLIOTHEK GOETTINGEN

TABLE 1 *Saccharomyces cerevisiae* strains used in this study

Strain name or description (laboratory reference no.)	Genotype	Reference or source
YPH499 (524, 776)	*MAT***a** *ade2-101 his3-Δ200 leu2-Δ1 ura3-52 trp1-Δ63 lys2-801*	60
mia40-3 (178)	*MAT***a** *ade2-101 his3-Δ200 leu2-Δ1 ura3-52 trp1-Δ63 lys2-801 mia40::ADE2* [pFL39-*FOMP2-8ts/mia40-3*]	34
mia40-4int (305)	*MAT***a** *ade2-101 his3-Δ200 leu2-Δ1 ura3-52 trp1-Δ63 lys2-801 mia40::MIA40-4* [*BG-fomp2-7-int-4-12*]	38
mia40-F311E (660)	*MAT***a** *ade2-101 his3-Δ200 leu2-1 ura3-52 trp1-63 lys2-801 mia40::ADE2* [pFL39-*MIA40-F311E*]	47
erv1-2 (235)	*MAT***a** *ade2-101 his3-Δ200 leu2-Δ1 ura3-52 trp1-Δ63 lys2-801 erv1::ADE2* [pFL39-*erv1-2*]	52
erv1-5 (318)	*MAT***a** *ade2-101 his3-Δ200 leu2-Δ1 ura3-52 trp1-Δ63 lys2-801 erv1::ADE2* [pFL39-*erv1-C159S*]	38
*mic19*Δ (762)	*MAT***a** *ade2-101 his3-Δ200 leu2-Δ1 ura3-52 trp1-Δ63 lys2-801 mic19::kanMX4*	This study
$Mic60_{ProtA}$ (493)	*MAT***a** *ade2-101 his3-Δ200 leu2-Δ1 ura3-52 trp1-Δ63 lys2-801* $mic60::MIC60_{ProtA}$	6
$Mic60_{ProtA}$ *mic19*Δ (686)	*MAT***a** *ade2-101 his3-Δ200 leu2-Δ1 ura3-52 trp1-Δ63 lys2-801* $mic60::MIC60_{ProtA}$ *mic19::kanMX4*	6
$Mia40_{His}$ (276)	*MAT***a** *ade2-101 his3-Δ200 leu2-Δ1 ura3-52 trp1-Δ63 lys2-801* $mia40::MIA40_{His10}$	47
$Mia40_{His}$ *mic19*Δ (763)	*MAT***a** *ade2-101 his3-Δ200 leu2-Δ1 ura3-52 trp1-Δ63 lys2-801* $mia40::MIA40_{His10}$ *mic19::kanMX4*	This study
$Erv1_{FLAG}$ (325)	*MAT***a** *ade2-101 his3-Δ200 leu2-Δ1 ura3-52 trp1-Δ63 lys2-801 erv1::ADE2* [pRS413-*Erv1-FLAG*]	This study
$Erv1_{FLAG}$ *mic19*Δ (799)	*MAT***a** *ade2-101 his3-Δ200 leu2-Δ1 ura3-52 trp1-Δ63 lys2-801 erv1::ADE2 mic19::kanMX4* [pRS413-*Erv1-FLAG*]	This study
tim17-5 (85)	*MAT***a** *ade2-101 his3-Δ200 leu2-Δ1 ura3-52 trp1-Δ63 lys2-801 tim17::TIM17-5* [*YPH-BG17-21-7*]	54
$Tom40_{C130/C138}$ (769)	*MAT***a** *ade2-101 his3-Δ200 leu2-Δ1 ura3-52 trp1-Δ63 lys2-801 tom40::ADE2* [pFL39-*TOM40-C165W/C326A/C341S/C355F/N130C/S138C*]	52
BY4741 (755)	*MAT***a** *his3Δ1 leu2Δ0 met15Δ0 ura3Δ0*	Euroscarf
*mic10*Δ (584)	*MAT***a** *his3Δ1 leu2Δ0 met15Δ0 ura3Δ0 mic10::kanMX4*	Euroscarf
*mic12*Δ (581)	*MAT***a** *his3Δ1 leu2Δ0 met15Δ0 ura3Δ0 mic12::kanMX4*	Euroscarf
*mic19*Δ (537)	*MAT***a** *his3Δ1 leu2Δ0 met15Δ0 ura3Δ0 mic19::kanMX4*	Euroscarf
*mic26*Δ (586)	*MAT***a** *his3Δ1 leu2Δ0 met15Δ0 ura3Δ0 mic26::kanMX4*	Euroscarf
*mic27*Δ (585)	*MAT***a** *his3Δ1 leu2Δ0 met15Δ0 ura3Δ0 mic27::kanMX4*	Euroscarf
*mic60*Δ (492, 834)	*MAT***a** *his3Δ1 leu2Δ0 met15Δ0 ura3Δ0 mic60::kanMX4*	Euroscarf
*tom5*Δ (569)	*MAT***a** *his3Δ1 leu2Δ0 met15Δ0 ura3Δ0 tom5::kanMX4*	Euroscarf
*tom70*Δ (633)	*MAT***a** *his3Δ1 leu2Δ0 met15Δ0 ura3Δ0 tom70::kanMX4*	Euroscarf

main is essential for the import of MIC19 into mitochondria. Human MIA40 was shown to interact in a redox-dependent manner with MIC19 and preferentially bind to Cys193 of MIC19 (41). Yeast Mic19 lacks the typical twin Cys-X_9-Cys motif. However, it contains two cysteine residues that are arranged in a single Cys-X_{10}-Cys motif that may serve as a simplified MIA substrate motif. Apart from the proposed role of human MIA40 in the maturation of MIC19, the oxidation state of both MIC19 in humans and Mic19 in yeast remains unknown.

Here, we determined the redox status of both human MIC19 and yeast Mic19 and systematically analyzed the role of the MIA pathway and MICOS complex in the biogenesis of Mic19. Furthermore, we elucidated the functional importance of Mic19 oxidation for its assembly into the MICOS complex. Finally, we investigated the role of Mic19 cysteine residues in the stability of the MICOS complex and, hence, the maintenance of mitochondrial morphology.

MATERIALS AND METHODS

Yeast strains and plasmids. The *S. cerevisiae* strains that were used in this study are listed in Table 1. To generate *mic19*Δ in the YPH499 background strain, the *kanMX4* cassette surrounded by the Mic19 promoter and terminator was amplified from the BY4741 background *mic19*Δ strain. Next, the cassette was introduced into strain YPH499 by homologous recombination according to a standard protocol. Oligonucleotide primers were designed to amplify the *MIC19* coding sequence together with native promoter and terminator and to clone it into the pRS416 vector, which gave rise to the pPS1 (153) plasmid. Cysteine-to-serine residue mutants of Mic19 were generated by site-directed mutagenesis using pPS1 as a template. This gave rise to plasmids carrying Mic19-C146S (pPS2, 154), Mic19-C157S (pPS3, 155), and Mic19-C146,157S (pPS4, 156). Plasmids with wild-type and cysteine-to-serine residue variants of Mic19 were transformed into YPH499 or BY4741 strains.

siRNA constructs and transfection. The targeting sequences used in this study were MIA40 (GGAAUGCAUGCAGAAAUAC [42]), ALR (GGAGUGUGCUGAAGACCUATT [43]), MIC60 (AAUUGCUGGAGCUGGCCUU [10]), and MIC10 (GCUUAUUCCAACUGUCAGCA). HeLa cells (20% confluence) were transfected with Oligofectamine (Invitrogen) in Opti-MEM medium (Gibco) with 250 nM small interfering RNA (siRNA) and after 4 h were supplemented with 0.5 volume of Dulbecco's modified Eagle medium containing 4.5 g/liter glucose, 10% fetal bovine serum, and 2 mM L-glutamine. Cells were cultured at 37°C in 5% CO_2 for 48 to 72 h. Custom and control nontargeting (Mission siRNA universal negative control; reference number SIC001; Sigma) duplex siRNAs were purchased from Sigma.

Mitochondrial procedures. Yeast cells were grown at 19 to 37°C on YPG medium (1% [wt/vol] yeast extract, 2% [wt/vol] Bacto peptone, 3% [wt/vol] glycerol) or YPS medium (1% [wt/vol] yeast extract, 2% [wt/vol] Bacto peptone, 2% [wt/vol] sucrose). To isolate mitochondria, differential centrifugation was used according to standard procedures (44). Isolated mitochondria were resuspended in SM buffer (250 mM sucrose, 10 mM MOPS [morpholinepropanesulfonic acid]-KOH [pH 7.2]) and stored at −80°C. Mitochondrial samples were prepared for electrophoresis by solubilization in dithiothreitol (DTT)-containing Laemmli buffer and denaturation at 65°C. Steady-state levels of mitochondrial proteins were assessed by SDS-PAGE under reducing conditions (50 mM DTT) and immunoblotting.

For proteinase K treatment, the isolated mitochondria were suspended in import buffer (250 mM sucrose, 80 mM KCl, 5 mM $MgCl_2$, 5 mM methionine, 10 mM KP_i, 10 mM MOPS-KOH [pH 7.2]). Proteinase K was added to a final concentration of 10 μg/ml and incubated with the mitochondria for 15 min on ice. The proteinase K activity was stopped by the addition of 2 mM phenylmethylsulfonyl fluoride (PMSF). Mitochondria were reisolated by centrifugation and analyzed by reducing SDS-PAGE followed by Western blotting.

For isolation of human mitochondria, human embryonic kidney 293 (HEK293) cells were cultured in Dulbecco's modified Eagle medium containing 1.8 g/liter galactose, 10% fetal bovine serum, and 2 mM L-glutamine at 37°C in 5% CO_2. Cells were harvested and homogenized in a Dounce homogenizer in isolation buffer (0.1% [wt/vol] bovine serum albumin [BSA], 300 mM trehalose, 10 mM HEPES-KOH, pH 7.7, 10 mM KCl, 1 mM EGTA, 1 mM EDTA, 2 mM PMSF) (45). The homogenate was cleared of cell debris by centrifugation at 1,000 × *g* for 10 min, and mitochondria were subsequently isolated by centrifugation at 10,000 × *g* for 15 min. The mitochondrial pellet was resuspended in isolation buffer without BSA.

Downloaded from http://mcb.asm.org/ on January 18, 2016 by NIEDERSAECHSISCHE STAATS- UND UNIVERSITAETSBIBLIOTHEK GOETTINGEN

Redox state analysis. To analyze the redox state of Mic19/MIC19, the isolated mitochondria were solubilized in Laemmli buffer either with 50 mM iodoacetamide (IA) or 15 mM 4-acetamido-4′-maleimidylstilbene-2,2′-disulfonic acid (AMS; Life Technologies) (nonreducing conditions) or with 50 mM DTT (reducing conditions) as a control. To characterize a redox form named $Mic19_{con}$, consisting of Mic19 conjugated to an unknown protein which is sensitive to mild reduction, a 15-min preincubation with 50 mM DTT in SM buffer at 20°C was performed before solubilization of the mitochondria in Laemmli buffer with 50 mM IA. To determine the oxidation status of human MIC19, indirect thiol trapping was performed. Isolated mitochondria were first incubated in isolation buffer without BSA containing 50 mM IA for 10 min at 37°C to block potential free cysteine residues. After centrifugation, the mitochondria were treated with isolation buffer containing 10 mM TCEP [Tris-(2-carboxyethyl)phosphine; Calbiochem] for 30 min to reduce the disulfide bonds and were subsequently solubilized in Laemmli buffer with 15 mM AMS. Proteins were separated on SDS-polyacrylamide gels followed by Western blotting.

To determine the redox state of human MIC19 in the total cell extract, cells were harvested and lysed in radioimmunoprecipitation assay (RIPA) buffer (65 mM Tris-HCl, pH 7.4, 150 mM NaCl, 1% [vol/vol] NP-40, 0.25% [wt/vol] sodium deoxycholate, 1 mM EDTA, 2 mM PMSF) containing 50 mM IA or 15 mM AMS to avoid shuffling of the disulfide bonds. After 30 min, the lysates were centrifuged at 14,000 × *g* for 30 min and the protein-containing supernatant was diluted with Laemmli buffer containing 50 mM IA or 15 mM AMS. A control total cell lysate was analyzed under reducing conditions (100 mM DTT).

Synthesis of precursor proteins and import into isolated mitochondria. Radiolabeled Mic19, Tim9, and Cox19 precursor proteins were synthesized using rabbit reticulocyte lysate (Promega) in the presence of [^{35}S]methionine (GE Healthcare) and 10 mM DTT, precipitated with ammonium sulfate, and denatured in urea buffer (8 M urea, 30 mM MOPS-KOH [pH 7.2], 50 mM DTT) (46). Radiolabeled F1β precursor was synthesized using a TNT quick coupled transcription/translation system (Promega). Where indicated, the mitochondria were pretreated with 1.6 mM methoxypolyethylene glycol maleimide (mPEG) for 30 min at 30°C and washed with SM buffer. The import of radiolabeled precursors into isolated mitochondria was performed at 30°C in import buffer (250 mM sucrose, 80 mM KCl, 5 mM $MgCl_2$, 5 mM methionine, 10 mM KP_i, 10 mM MOPS-KOH [pH 7.2]) supplemented with 3% fatty acid-free bovine serum albumin in the case of Mic19 and F1β import. To dissipate the electrochemical IM potential, the import of Mic19 was performed in the presence of 8 μM antimycin A, 1 μM valinomycin, 20 μM oligomycin (VOA) unless indicated otherwise. The precursor was added to the reaction mixture. The import was stopped by the addition of 50 mM iodoacetamide or VOA and incubation on ice. To remove the nonimported precursor, mitochondria were incubated with proteinase K (50 μg/ml) for 15 min. The proteinase K activity was stopped by the addition of 2 mM PMSF. Next, the samples were washed with SM buffer and analyzed under reducing conditions on SDS-polyacrylamide gels followed by autoradiography. The efficiency of protein import was determined by densitometry of the autoradiography images with the use of the ImageQuantTL program followed by quantification. The amount of protein imported into the mitochondria of the wild-type strain at the time points indicated below was set equal to 100%. The results of three independent experiments were analyzed. The line graphs show mean and standard error of the mean (SEM) values.

Affinity purification of $Mic60_{ProtA}$ from isolated mitochondria. Mitochondria (1 to 2 mg) isolated from yeast cells expressing protein A-tagged Mic60 ($Mic60_{ProtA}$) were incubated in solubilization buffer (1% [wt/vol] digitonin, 20 mM Tris, pH 7.4, 50 mM NaCl, 0.5 mM EDTA, 10% [vol/vol] glycerol, 50 mM IA, 2 mM PMSF) for 20 min on ice. Where indicated, DTT pretreatment of the mitochondria for 15 min at 20°C (SM buffer containing 50 mM DTT) was performed. After solubilization, extracts were clarified by centrifugation and incubated with preequilibrated immunoglobulin G (IgG)-Sepharose beads (GE Healthcare) for 2 h. Next, the beads were washed three times with wash buffer (20 mM Tris, pH 7.4, 50 mM NaCl, 0.5 mM EDTA, 10% [vol/vol] glycerol, 50 mM IA, 2 mM PMSF). The bound fraction was eluted by incubation with Laemmli buffer containing 50 mM DTT or 50 mM IA. The efficiency of coisolation of wild-type Mic19 and Mic19 cysteine-to-serine variants with $Mic60_{ProtA}$ was determined by Western blotting and quantified with the use of ImageQuantTL. The relative amounts of Mic19 variants that eluted with $Mic60_{ProtA}$ were calculated and normalized both to the amount of Mic19 in the load fraction and to the efficiency of $Mic60_{ProtA}$ purification. The amount of wild-type Mic19 that eluted with $Mic60_{ProtA}$ was set equal to 1. The efficiencies of coisolation of other MICOS proteins with $Mic60_{ProtA}$ were calculated from the quantified signals from the eluate fraction and corrected for the efficiency of $Mic60_{ProtA}$ purification. The amounts of proteins coisolated with $Mic60_{ProtA}$ in the presence of wild-type Mic19 were set equal to 1, and the other results are shown as the fold changes.

Affinity purification of $Mia40_{His}$ from isolated mitochondria. The affinity purification of carboxy-terminal His_{10}-tagged Mia40 ($Mia40_{His}$) was performed according to the procedure described previously (47). Mitochondria isolated from yeast (1 mg) with $Mia40_{His}$ were incubated in solubilization buffer S (1% [wt/vol] digitonin, 10% [wt/vol] glycerol, 20 mM Tris, pH 7.4, 150 mM NaCl, 20 mM imidazole, 50 mM IA, 2 mM PMSF) for 20 min on ice. After solubilization, extracts were clarified by centrifugation and subjected to incubation with Ni-nitrilotriacetic acid-agarose beads (Qiagen) for 1 h. Next, the beads were washed twice with buffer W (20 mM Tris, pH 7.4, 150 mM NaCl, 20 mM imidazole). The bound fraction was eluted with buffer E (20 mM Tris, pH 7.4, 100 mM NaCl, 400 mM imidazole, 50 mM IA) and analyzed by reducing or nonreducing SDS-PAGE followed by Western blotting.

Affinity purification of $Erv1_{FLAG}$ from cell extracts. Yeast cells expressing carboxy-terminal FLAG-tagged Erv1 ($Erv1_{FLAG}$) were grown at 19°C overnight on YPG medium to the mid-log phase. The affinity purification of $Erv1_{FLAG}$ was performed according to the procedure described previously (40). Yeast cells were harvested by centrifugation and resuspended in buffer F (20 mM Tris, pH 7.4, 300 mM NaCl, 50 mM IA). The cells were lysed with a French press (CD-019 disruption system; Constant Cell) under a pressure of 214 MPa followed by solubilization of the extracts for 20 min in digitonin-containing buffer (1% [wt/vol] digitonin, 20 mM Tris, pH 7.4, 300 mM NaCl, 50 mM IA, 2 mM PMSF). After a clarifying spin, the extracts were subjected to an anti-FLAG M2 affinity gel (Sigma-Aldrich) for 2 h at 4°C. After three washes with buffer F, the proteins were eluted in Laemmli buffer with 50 mM DTT or 50 mM IA. The eluted proteins were analyzed by reducing or nonreducing SDS-PAGE followed by Western blotting.

Electron microscopy of yeast cells. For electron microscopy, the yeast cells were grown at 30°C in selective liquid medium containing 3% glycerol and 0.1% glucose (6.7 g/liter yeast nitrogen base, 2 g/liter dropout mix without uracil [48], 30 ml/liter glycerol, 1 g/liter glucose) and harvested in the logarithmic growth phase. The yeast cells were fixed for 20 min in 1.5% potassium permanganate as previously described (49) and poststained with 1% uranyl acetate for 2 h. After dehydration in a graded ethanol series and propylene oxide, the cells were embedded in epoxide resin (Agar 100; Plano, Wetzlar, Germany). Ultrathin sections were examined using a Philips CM 120 transmission electron microscope (Philips, Eindhoven, Netherlands), and images were taken with a TemCam F416 complementary metal oxide semiconductor (CMOS) camera (Tietz Video and Image Processing Systems GmbH, Gauting, Germany).

Miscellaneous. SDS-PAGE was performed using standard procedures. Proteins were separated on 15% polyacrylamide gels. Polyvinylidene difluoride membranes (Millipore) were used for Western blotting. An enhanced chemiluminescence detection system was used, and chemiluminescence was detected with X-ray films (Foton-Bis). Radioactively labeled proteins were visualized by digital autoradiography (Storm imaging system; GE Healthcare), followed by image processing with ImageQuant software (GE Healthcare). The protein concentration was determined by the Bradford method using the Roti-Quant reagent (Carl Roth GmbH) and bovine serum albumin as the protein standard.

Downloaded from http://mcb.asm.org/ on January 18, 2016 by NIEDERSAECHSISCHE STAATS- UND UNIVERSITAETSBIBLIOTHEK GOETTINGEN

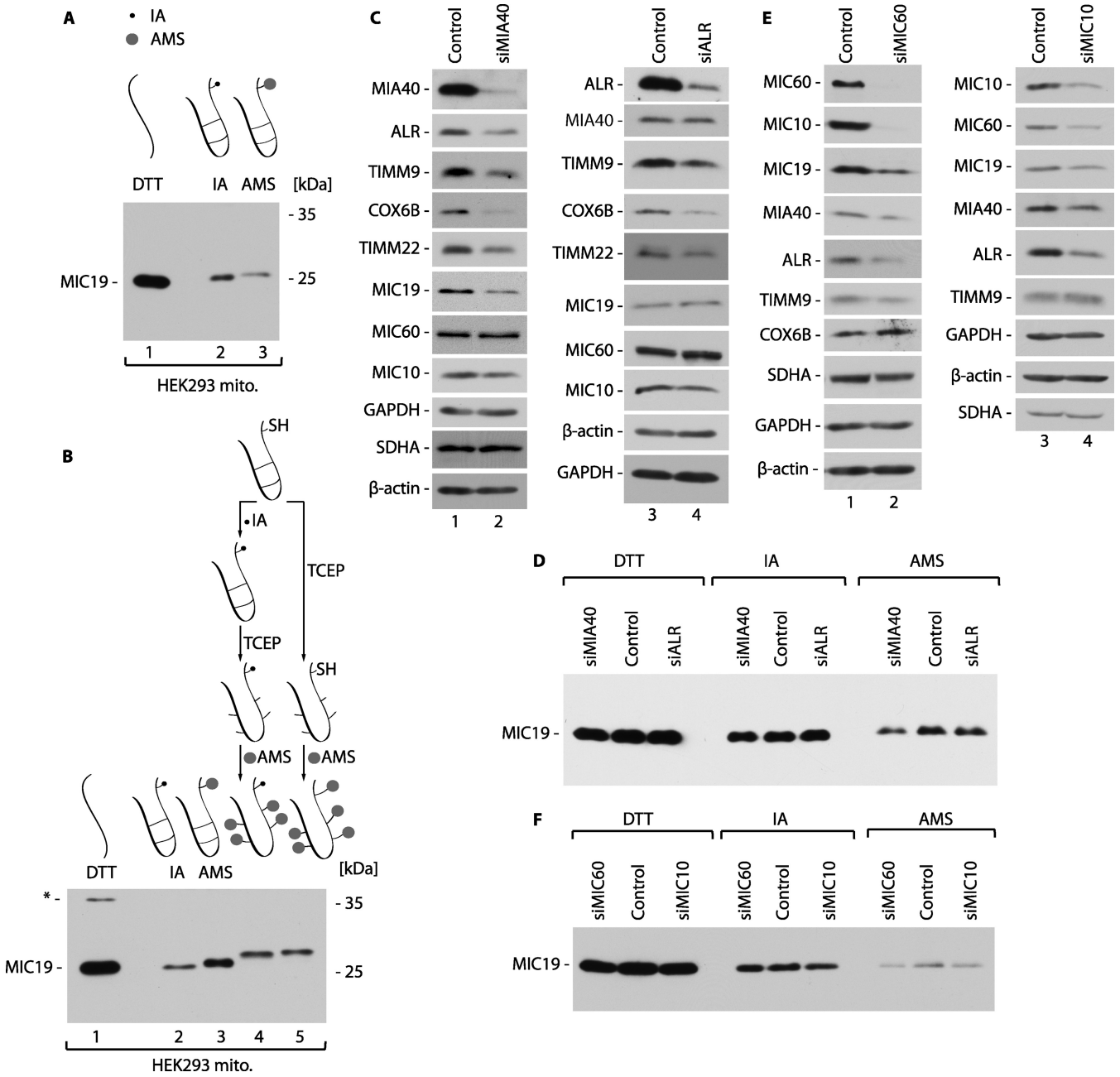

FIG 1 Human MIC19 forms two disulfide bonds. (A) Mitochondria isolated from HEK293 cells (HEK203 mito.) were analyzed by reducing (DTT) or nonreducing SDS-PAGE. Under nonreducing conditions, free cysteine residues were modified by IA or AMS. (B) Mitochondria isolated from HEK293 cells were subjected to indirect thiol trapping. The schema of the experiment is provided at the top. Asterisk, an unspecific signal. (C) Cellular protein extracts from HeLa cells were analyzed 72 h after transfection with siRNA targeting MIA40 (siMIA40) or ALR (siALR). Samples were analyzed by reducing (DTT) SDS-PAGE. GAPDH, glyceraldehyde-3-phosphate dehydrogenase. (D) Cellular protein extracts from HeLa cells were analyzed 48 h after transfection with siRNA targeting MIA40 or ALR. Samples were analyzed by reducing (DTT) and nonreducing SDS-PAGE. Under nonreducing conditions, free cysteine residues were modified by IA or AMS. (E and F) Cellular protein extracts from HeLa cells were analyzed 72 h after transfection with siRNA targeting MIC60 (siMIC60) or MIC10 (siMIC10). Samples were analyzed by reducing (DTT) SDS-PAGE (E) or by reducing (DTT) and nonreducing SDS-PAGE (F). Under nonreducing conditions, free cysteine residues were modified by IA or AMS.

RESULTS

Human MIC19 forms two disulfide bonds in the CHCH domain, and its mitochondrial localization depends on the MIA pathway. MIC19 interacts with human MIA40, creating a disulfide bridge between Cys193 of MIC19 and redox-active Cys55 of MIA40 (41). The mode of this interaction suggests that MIC19 may undergo oxidative folding (41). However, the redox status of MIC19 has not been studied. We analyzed the redox state of native MIC19 in isolated mitochondria of HEK293 cells (Fig. 1A). We treated mitochondria with the reducing agent DTT and cysteine residue-blocking agents IA and AMS and analyzed the migration of the MIC19 protein. MIC19 migrated slightly differently under

Downloaded from http://mcb.asm.org/ on January 18, 2016 by NIEDERSAECHSISCHE STAATS- UND UNIVERSITAETSBIBLIOTHEK GOETTINGEN

reducing conditions (DTT) than under nonreducing conditions (IA) (Fig. 1A, lanes 1 and 2). This change in migration can be caused by protein oxidation. We also observed a further change in MIC19 migration when mitochondria were treated with AMS, which irreversibly binds to reduced cysteine residues and adds 0.5 kDa to the protein mass (Fig. 1A, lanes 2 and 3). Based on this migration pattern, we hypothesized that AMS bound to only 1 cysteine residue and that 4 other cysteine residues form disulfide bonds. Under nonreducing conditions, especially upon AMS treatment, the MIC19 signal intensity was noticeably reduced, likely due to altered antibody recognition (Fig. 1A).

To further test the hypothesis regarding MIC19 oxidation, we applied the indirect thiol trap assay (Fig. 1B). Mitochondria isolated from HEK293 cells were first incubated with IA to irreversibly block the free cysteine residues. The mitochondria were then treated with TCEP to reduce the disulfide-bonded cysteine residues, and the mitochondria were then incubated with AMS. This resulted in the binding of AMS molecules to cysteine residues that were oxidized under native conditions (Fig. 1B, lane 4). MIC19 from such a treated sample migrated on the SDS-polyacrylamide gel more slowly than MIC19 from a sample treated only with AMS (Fig. 1B, compare lanes 4 and 3), demonstrating the oxidation of MIC19. As an additional control, the mitochondrial sample was reduced with TCEP and subsequently incubated with AMS without prior blocking with IA. Under these conditions, AMS bound to all cysteine residues of MIC19. As a result, MIC19 migrated slightly more slowly than it did when prior IA blocking was applied (Fig. 1B, compare lanes 5 and 4). This confirmed that native MIC19 forms two disulfide bonds and has one additional reduced cysteine residue.

MIC19 cysteine residues were previously shown to be needed for interactions with MIA40 (41). Using siRNA, we knocked down the expression of the MIA pathway proteins MIA40 and ALR (the human homolog of yeast Erv1) to determine their involvement in the biogenesis of MIC19 (Fig. 1C). Upon knockdown of MIA40, the levels of ALR, TIMM9, and COX6B were reduced. The yeast homologues of these well-conserved cysteine-rich proteins of the IMS are known to be the MIA transport substrates (34, 36, 38). Also, the levels of TIMM22, the recently reported noncanonical MIA pathway substrate protein in yeast (47), were decreased (Fig. 1C, lanes 1 and 2). Interestingly, the levels of MIC19 were also significantly reduced, indicating a role for MIA40 in its transport (Fig. 1C, lanes 1 and 2). When ALR was knocked down, TIMM9, COX6B, and TIMM22 levels were decreased, but no effect on MIC19 was observed (Fig. 1C, lanes 3 and 4). We tested if other MICOS components are affected upon knockdown of the MIA pathway components. The levels of MIC60 remained unchanged, whereas the levels of MIC10 were slightly reduced after silencing of both MIA40 and ALR (Fig. 1C, lanes 1 to 4). We further analyzed the redox state of MIC19 in MIA pathway-deficient cells. No defect in MIC19 oxidation was observed after siRNA transfection (Fig. 1D). Thus, the MIA pathway is involved in maintaining the MIC19 levels. The successfully imported molecules of Mic19 were found in an oxidized state.

We also analyzed the influence of MICOS deficiency on MIC19 protein levels and the redox state. The effect of MIC60 downregulation on other MICOS components, including MIC19, was recently shown (16). After transfection with siRNA that targeted MIC60 or MIC10, we observed the downregulation of MIC60 and MIC10 in both cases, confirming their interdependence (Fig. 1E, lanes 1 to 4). Both MIC60 and MIC10 knockdown resulted in a moderate reduction of MIC19 levels (Fig. 1E). Additionally, we observed that MIC60 and MIC10 knockdown resulted in downregulation of the levels of MIA40 and ALR. This points to an interdependence of MIA on the MICOS complex reported for yeast (6). No difference in the MIC19 redox state was observed upon MIC60 or MIC10 depletion (Fig. 1F). Thus, we conclude that the levels but not the redox state of MIC19 depend on MIA40 and the MICOS complex.

Import of yeast Mic19 into mitochondria is dependent on the MIA pathway. Yeast Mic19 is shorter than its human counterpart and possesses a single atypical Cys-X_{10}-Cys motif, which differs from the classic motifs of MIA pathway substrates (Fig. 2A). We analyzed whether the cysteine residues of yeast Mic19 are oxidized in mitochondria similarly to human MIC19. The redox state analysis showed that the migration of Mic19 on SDS-polyacrylamide gels differed between nonreducing conditions and reducing conditions with DTT (Fig. 2B). To provide further evidence, we irreversibly modified the putative thiol groups of cysteine residues with AMS. The AMS treatment did not change the migration of native Mic19, indicating that the protein is indeed oxidized (Fig. 2B). Furthermore, we generated single (C146S and C157S) and double (C146,157S) cysteine-to-serine substitution mutants of Mic19 and analyzed their migration under nonreducing conditions. As expected, the cysteine mutants migrated more slowly than the oxidized, wild-type Mic19 (Fig. 2C). Thus, the difference in migration was attributable to Mic19 oxidation.

MIA is the only pathway that is known to be responsible for protein oxidation in mitochondria. Classically, Mia40 drives the coupled import and oxidation of proteins of the IMS (29, 33). Recent studies demonstrated the involvement of the MIA pathway in the oxidation and assembly of noncanonical protein substrates, including the integral inner membrane protein Tim22 (47), the inner membrane-associated IMS protein Atp23 (50), and the matrix protein Mrp10 (51). To test whether Mia40 is involved in the biogenesis of yeast Mic19, we used temperature-sensitive conditional mutant strains of Mia40 (34, 38, 47). We analyzed the steady-state levels of proteins in mitochondria that were isolated from *mia40-3*, *mia40-4int*, and *mia40*-F311E mutants that were grown at a restrictive temperature (37°C). The levels of the classic MIA pathway substrates Tim10 and Cox12 were markedly decreased in all the analyzed mutants compared with those in wild-type cells (Fig. 2D). We noticed a significant reduction of Mic19 levels, but this decrease was not as severe as that in the case of the classic substrates (Fig. 2D). Other control mitochondrial proteins (including another MICOS component, Mic10) remained unaffected (Fig. 2D). We also determined whether Erv1, a partner of Mia40, influenced Mic19 biogenesis. Like the Mia40 mutants, Erv1 conditional mutants (38, 52) exhibited a decrease in the levels of Mic19 in mitochondria, although the decrease was minor in the *erv1-5* mutant (Fig. 2E). The levels of Mic60 and Mic10 were also slightly decreased, suggesting an additional link between MIA and MICOS components other than Mic19. As expected, the classic MIA substrates Tim10, Pet191, and Ccs1 were significantly downregulated, whereas other control proteins from all mitochondrial compartments were unaffected (Fig. 2E).

Next, using the radiolabeled [^{35}S]Mic19 precursor protein, we performed *in organello* import into mitochondria to analyze the biogenesis of Mic19. We analyzed the import of Mic19 into mitochondria that were isolated from the MIA pathway mutants

Downloaded from http://mcb.asm.org/ on January 18, 2016 by NIEDERSAECHSISCHE STAATS- UND UNIVERSITAETSBIBLIOTHEK GOETTINGEN

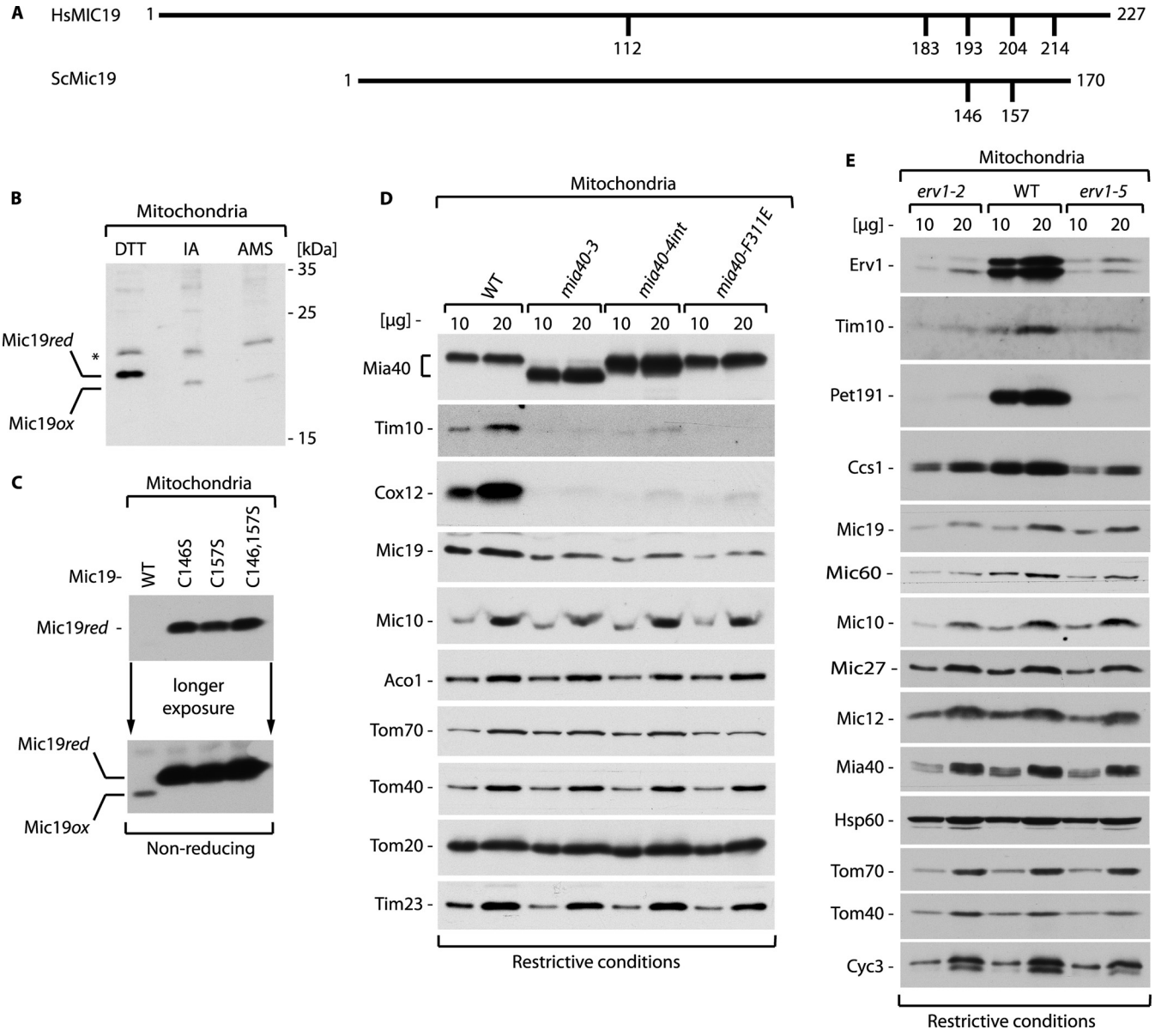

FIG 2 The MIA pathway is involved in the biogenesis of Mic19. (A) Schematic presentation of human MIC19 and yeast Mic19 proteins. The positions of cysteine residues are marked. HsMIC19, *Homo sapiens* MIC19; ScMic19, *Saccharomyces cerevisiae* Mic19. (B) Mitochondria isolated from wild-type yeast cells were analyzed by reducing (DTT) or nonreducing SDS-PAGE. Under nonreducing conditions, free cysteine residues were modified by iodoacetamide or AMS. ox, oxidized; red, reduced; asterisk, an unspecific signal. (C) (Top) Mitochondria isolated from yeast strains expressing wild-type (WT) or cysteine mutants of the Mic19 protein were analyzed by nonreducing SDS-PAGE in the presence of iodoacetamide. (Bottom) A longer exposure of the same experiment shown at the top. (D and E) Protein levels in mitochondria isolated from the indicated yeast strains shifted to 37°C for 8 h (D) or 7 h (E) are shown. The samples were analyzed by reducing SDS-PAGE.

grown under permissive conditions. We observed that the efficiency of Mic19 import decreased in the *mia40-3* mutant compared with that in the wild type (Fig. 3A). The import efficiency also decreased in the mitochondria from the *erv1-2* and *erv1-5* mutants, and the effect was even more pronounced than that in the case of the *mia40-3* mutant (Fig. 3B and C). Thus, the import of Mic19 was decreased up to 50% in the MIA pathway mutants, whereas the level of import of the classic MIA pathway substrates Tim9 and Cox19 was decreased to approximately 10 to 20% of the level for the wild type (Fig. 3D to F), in agreement with the findings presented in the literature (30, 34, 36, 38). These observations indicate that the MIA pathway plays a role in promoting the efficient accumulation of Mic19 in mitochondria.

Other requirements for mitochondrial import of Mic19. We analyzed the role of the TOM complex in Mic19 translocation. Radiolabeled Mic19 was imported into mitochondria isolated from *tom5*Δ and *tom70*Δ yeast strains, and a decrease in the import efficiency compared with that for the wild type was observed (Fig. 4A). Next, we imported Mic19 into the mitochondria isolated from yeast that express Tom40 with cysteines at positions 130 and 138 ($Tom40_{C130/C138}$). The $Tom40_{C130/C138}$ variant enables the blockade of the TOM translocase channel by modifica-

Downloaded from http://mcb.asm.org/ on January 18, 2016 by NIEDERSAECHSISCHE STAATS- UND UNIVERSITAETSBIBLIOTHEK GOETTINGEN

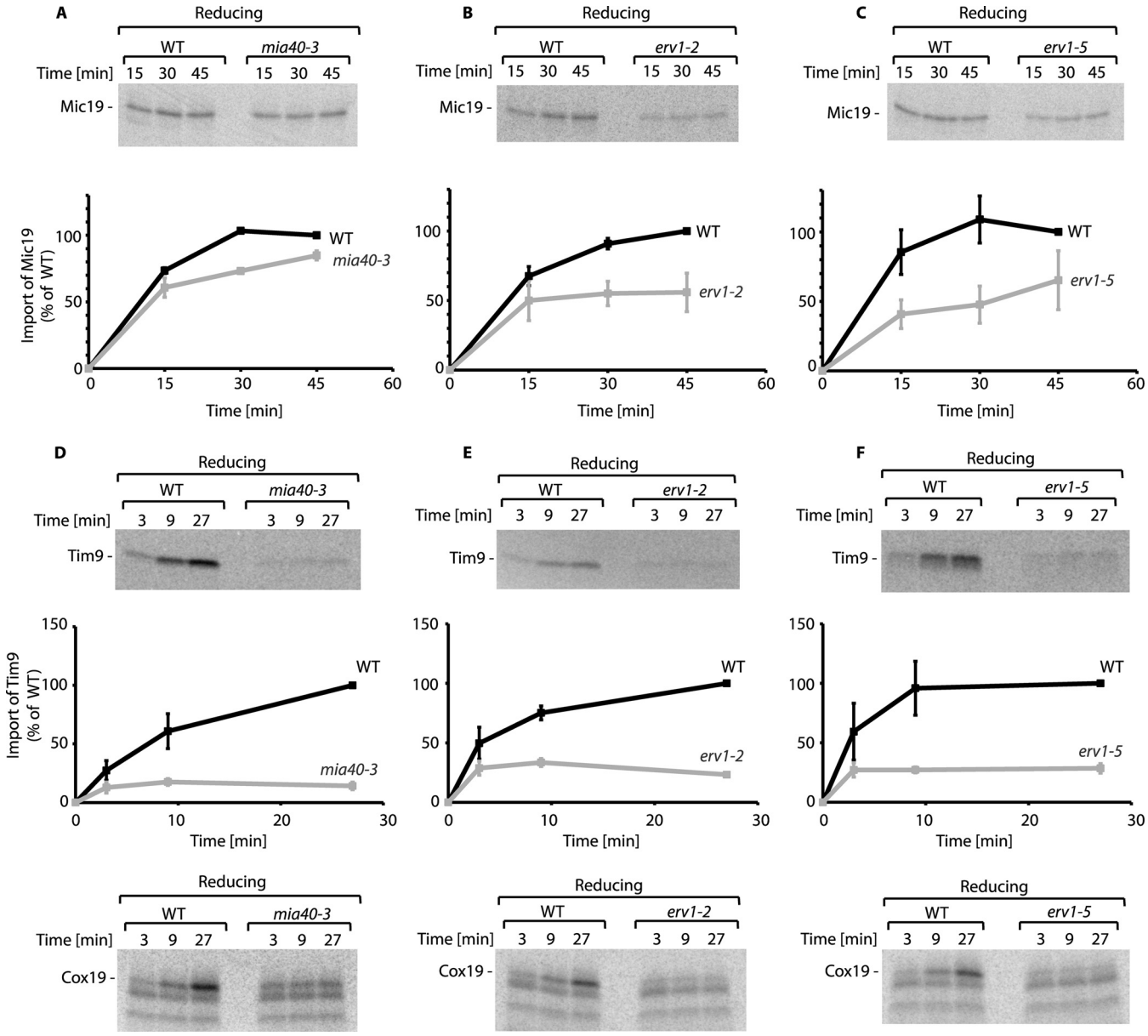

FIG 3 Import of yeast Mic19 depends on the MIA pathway. (A to C) Radiolabeled [^{35}S]Mic19 protein precursor was imported into mitochondria isolated from yeast grown at 19°C. Quantifications of the import efficiency are shown as graphs at the bottom of each panel. The level of import into wild-type mitochondria after 45 min was set equal to 100%. (D to F) Radiolabeled [^{35}S]Tim9 or [^{35}S]Cox19 protein precursor was imported into mitochondria isolated from yeast grown at 19°C. Quantifications of the Tim9 import efficiency are shown as graphs at the bottom of each panel. The level of import into wild-type mitochondria after 27 min was set equal to 100%. Means from three independent experiments are shown. Error bars indicate standard errors of the means. WT, wild type. Samples were analyzed by reducing SDS-PAGE and autoradiography.

tion with an alkylating agent, mPEG (52, 53). The $Tom40_{C130/C138}$ variant was efficiently modified with mPEG (Fig. 4B). As a control, Cyc3, which possesses accessible cysteine residues, was also modified by mPEG; in contrast, the cysteine residues of Mic19 and Cox12 are engaged in the disulfide bonds and are thus protected from mPEG binding (Fig. 4B). After blocking with mPEG, Mic19 import was decreased in the $Tom40_{C130/C138}$ variant (Fig. 4C), demonstrating that the TOM complex is the entry for Mic19 into mitochondria.

The increased import of Mic19 upon dissipation of the electrochemical IM potential was observed (Fig. 4D). This is in contrast to the findings for presequence-carrying proteins (24–27). We imported radiolabeled Mic19 into the mitochondria isolated from the *tim17-5* mutant, which is defective in the import of proteins via the presequence-dependent TIM23 pathway (24–27, 54). Interestingly, Mic19 was imported into the *tim17-5* mutant mitochondria even more efficiently than into the wild-type mitochondria (Fig. 4E) regardless of whether the electrochemical IM potential was dissipated or not. As expected, the import of the control presequence-containing protein, F1β, was inhibited in *tim17-5* mutant mitochondria (Fig. 4F). These data do not support the role of the TIM23 pathway in Mic19 import.

Downloaded from http://mcb.asm.org/ on January 18, 2016 by NIEDERSAECHSISCHE STAATS- UND UNIVERSITAETSBIBLIOTHEK GOETTINGEN

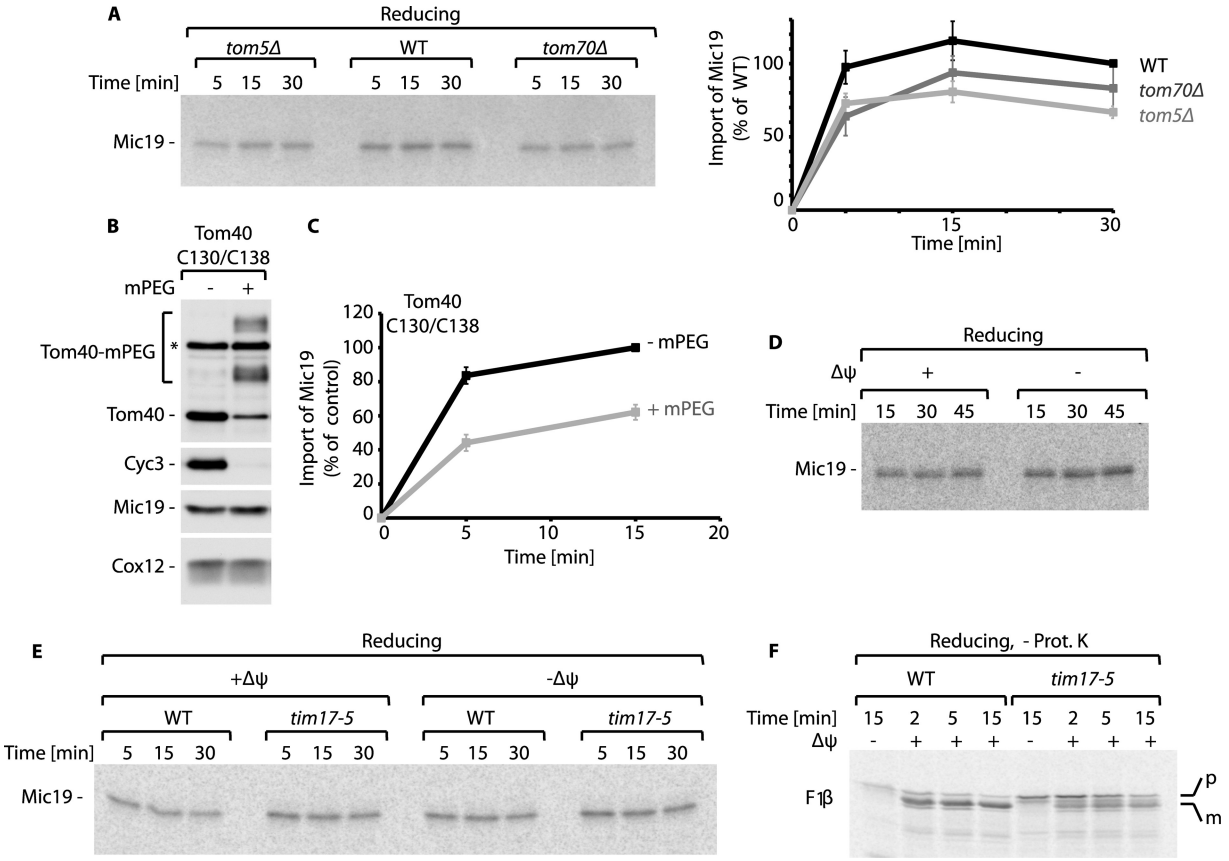

FIG 4 Mic19 enters mitochondria through the TOM complex. (A) Radiolabeled [^{35}S]Mic19 protein precursor was imported into mitochondria isolated from yeast grown at 19°C. Quantification of the import efficiency is shown as a graph on the right. The level of import into wild-type mitochondria after 30 min was set equal to 100%. (B) The protein levels of mitochondria carrying Tom40$_{C130/C138}$ after treatment with mPEG were analyzed by reducing SDS-PAGE followed by Western blotting. Asterisk, an unspecific signal. (C) Quantification of the import of Mic19 into mitochondria carrying Tom40$_{C130/C138}$ with or without blockade by mPEG. The level of import into untreated mitochondria after 15 min was set equal to 100%. Means from three independent experiments are shown. Error bars indicate standard errors of the means. (D) Radiolabeled [^{35}S]Mic19 protein precursor was imported into mitochondria isolated from yeast grown at 19°C. The electrochemical IM potential was dissipated, as indicated. (E) Radiolabeled [^{35}S]Mic19 protein precursor was imported into mitochondria isolated from yeast grown at 19°C. The electrochemical IM potential was dissipated where indicated. (F) Radiolabeled [^{35}S]F$_1$β protein precursor was imported into mitochondria isolated from yeast grown at 19°C. Samples were analyzed by reducing SDS-PAGE and autoradiography. Prot. K, proteinase K; WT, wild type; Δψ, electrochemical membrane potential.

The redox state of Mic19 does not influence its mitochondrial localization. It was shown for other proteins, including Mia40 (30, 55), that different redox states can be distinguished under mild reducing conditions. We applied mild reducing conditions (DTT at 20°C) and found that only a fraction of Mic19 migrated more slowly than oxidized Mic19 (Mic19$_{ox}$) under nonreducing conditions (Fig. 5A, compare lanes 2 and 1). Interestingly, we also found that although this form of Mic19 appeared, the lower band that represented the oxidized form (Mic19$_{ox}$) did not disappear unless it was reduced under harsh conditions (Fig. 5A; compare lane 2 and lanes 3 and 4). This suggests that the appearance of the upper band resulted from a disruption of the high-molecular-mass disulfide-bonded intermolecular conjugate of Mic19 with an unknown protein which is sensitive to mild reduction (Fig. 5B). Hereinafter we refer to this form as the Mic19 conjugate (Mic19$_{con}$). Because the antibody against Mic19 recognizes numerous nonspecific signals (not shown), we were unable to directly observe the high-molecular-mass conjugate. Thus, in the following experiments, we analyzed the intermolecular conjugate by observing the Mic19$_{con}$ form upon mild reduction.

The cysteine variants were present in mitochondria at levels similar to those of wild-type Mic19 (Fig. 5C). The localization of Mic19 cysteine mutants inside mitochondria was further confirmed by protease treatment of the isolated mitochondrial fraction (Fig. 5D). Interestingly, despite the dependence of Mic19 on the MIA pathway, the cysteine residues that created a disulfide bond were not required for mitochondrial localization (Fig. 5C and D). Thus, chaperoning rather than disulfide bond transfer seemed to be a dominant MIA function for Mic19, a finding similar to that for other noncanonical MIA substrates (47, 50). As expected, all three mutants were unable to form the intramolecular disulfide bond of Mic19$_{ox}$, as they migrated at the height of reduced Mic19 (Mic19$_{red}$)/Mic19$_{con}$ (Fig. 5E). The signal observed from wild-type Mic19 analyzed under nonreducing conditions was much weaker than that from wild-type Mic19 analyzed under reducing conditions (Fig. 5E; also Fig. 2A) due to the fact that a portion of Mic19 was engaged in the formation of Mic19$_{con}$. The signals from the Mic19 cysteine mutants did not differ between reducing and nonreducing conditions, suggesting that these cysteine variants are unable to form Mic19$_{con}$. We further

Downloaded from http://mcb.asm.org/ on January 18, 2016 by NIEDERSAECHSISCHE STAATS- UND UNIVERSITAETSBIBLIOTHEK GOETTINGEN

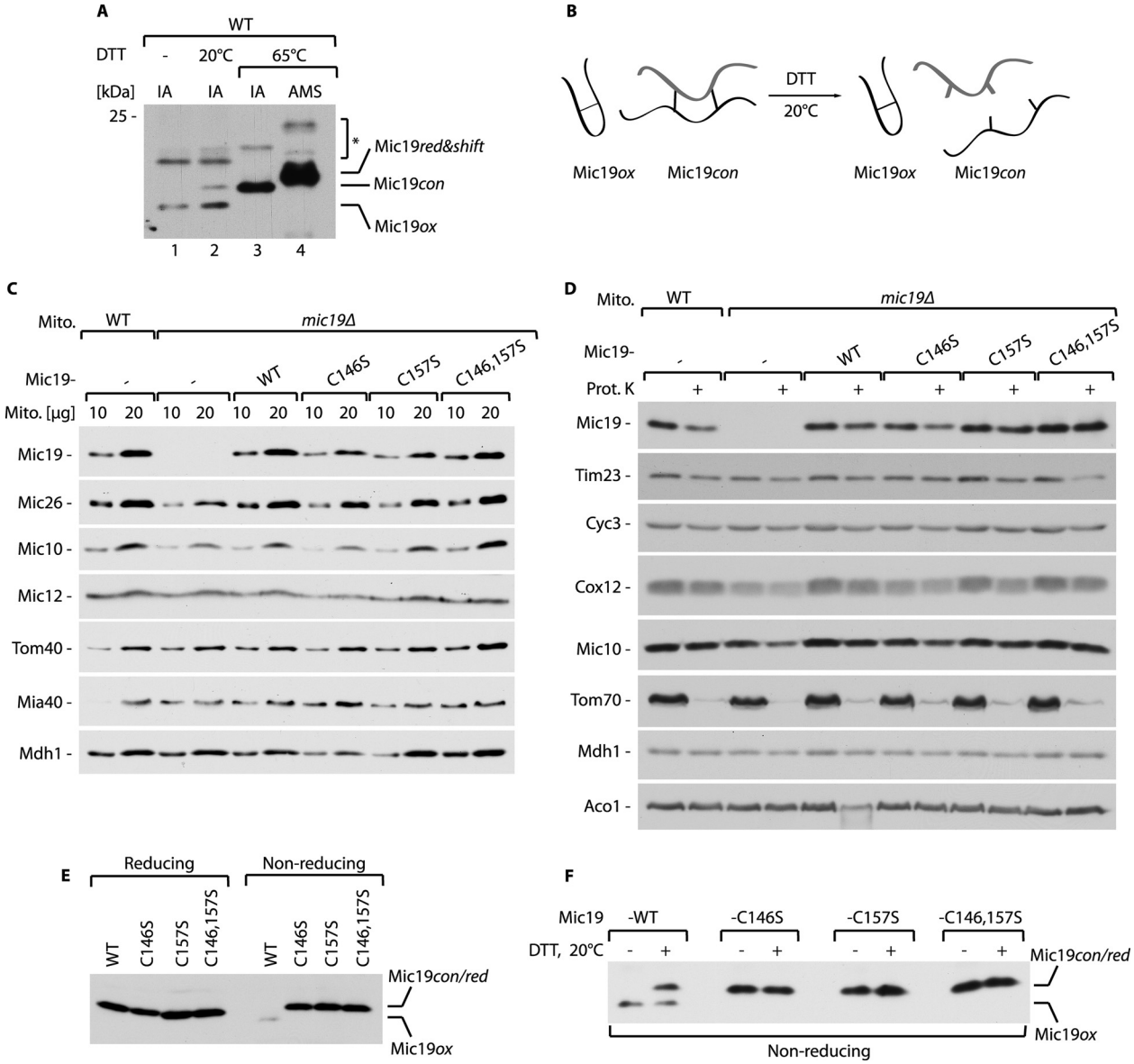

FIG 5 Mic19 forms a disulfide-bonded conjugate. (A) Mitochondria isolated from wild-type yeast were incubated with IA or AMS to block the free sulfhydryl groups of cysteine residues. Where indicated, pretreatment with DTT (20°C with mild reducing conditions or 65°C with harsh reducing conditions) was performed. Samples were analyzed by nonreducing SDS-PAGE followed by Western blotting. ox, oxidized; red&shift, reduced and shifted by AMS; con, conjugate; asterisk, unspecific signals. (B) A schematic model of the proposed Mic19 redox forms. (C) The protein levels of mitochondria isolated from wild-type and *mic19*Δ yeast strains carrying the indicated variants of the Mic19 protein or the empty vector as a control grown at 19°C are shown. The samples were analyzed by reducing SDS-PAGE followed by Western blotting. (D) Mitochondria isolated from the indicated yeast strains were incubated with proteinase K. Samples were analyzed by reducing SDS-PAGE followed by Western blotting. (E) Mitochondria isolated from a *mic19*Δ yeast strain expressing the wild-type or mutant Mic19 protein were analyzed under reducing or nonreducing conditions. (F) Mitochondria isolated from a *mic19*Δ yeast strain expressing the wild-type or mutant Mic19 protein were incubated with IA to block the free sulfhydryl groups of cysteine residues. Where indicated, pretreatment under mild reducing conditions (DTT, 20°C) was performed. Samples were analyzed by nonreducing SDS-PAGE followed by Western blotting. WT, wild type.

sought to determine whether and which cysteine residues are required for the formation of a Mic19 conjugate that is represented by $Mic19_{con}$. To investigate this experimentally, we pretreated isolated mitochondria that carried wild-type and cysteine variants of Mic19 with DTT and observed no difference in the amounts of the $Mic19_{red}$/$Mic19_{con}$ signal seen under mild reducing conditions and those seen with no treatment (Fig. 5F). If a cysteine mutant was able to form this conjugate, then the mild reducing conditions would cause its disruption, leading to an increase in the levels of the signals observed (the $Mic19_{red}$ and $Mic19_{con}$ signals) compared with those observed with untreated samples. Such an increase was not observed for any of the analyzed mutants (Fig. 5F). Thus, none of the cysteine variants of Mic19 were able to form the conjugate. We concluded that both cysteine residues of Mic19 are needed for intermolecular conjugate stability, in line with the schematic model (Fig. 5B).

The MIA pathway is not required for trapping oxidized Mic19. We analyzed the redox state of Mic19 in the conditional

Downloaded from http://mcb.asm.org/ on January 18, 2016 by NIEDERSAECHSISCHE STAATS- UND UNIVERSITAETSBIBLIOTHEK GOETTINGEN

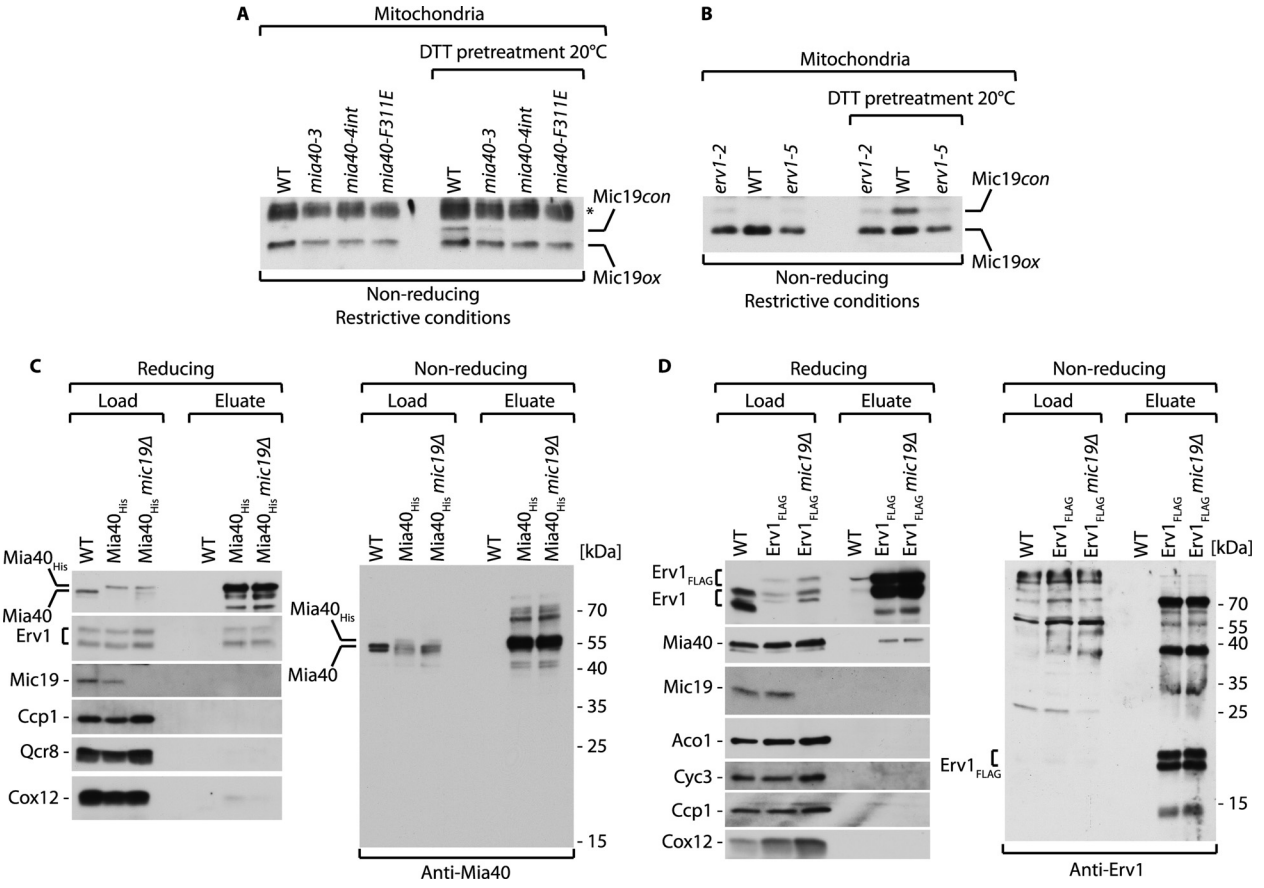

FIG 6 The generation of the Mic19 conjugate is dependent on the MIA pathway. (A and B) Mitochondria isolated from the conditional MIA pathway mutant strains shifted to 37°C for 8 h (A) or 7 h (B) were incubated with IA to block the free sulfhydryl groups of cysteine residues. Where indicated, pretreatment under mild reducing conditions (DTT, 20°C) was performed. Samples were analyzed by nonreducing SDS-PAGE followed by Western blotting. ox, oxidized; con, conjugate; asterisk, an unspecific signal. (C) Mitochondria isolated from the wild-type strain, a strain expressing $Mia40_{His}$, and a *mic19*Δ strain expressing $Mia40_{His}$ were solubilized, and affinity purification of $Mia40_{His}$ was performed. Samples were analyzed by reducing (left) or nonreducing (right) SDS-PAGE followed by immunodecoration. Load, 2%; eluate, 100%. (D) After yeast cell disruption, extracts from the wild-type strain, a strain expressing $Erv1_{FLAG}$, and a *mic19*Δ strain expressing $Erv1_{FLAG}$ were subjected to affinity purification. Samples were analyzed by reducing (left) or nonreducing (right) SDS-PAGE followed by immunodecoration. Load, 1%; eluate, 100%; WT, wild type.

mutants of Mia40 that were grown at a restrictive temperature. We observed a slight decrease in the levels of oxidized Mic19 under nonreducing conditions (Fig. 6A). However, when we applied mild reducing conditions, the $Mic19_{con}$ signal appeared in the wild type but was strongly decreased or completely absent in the Mia40 mutants (Fig. 6A). These results show that Mia40 is involved in the formation of the conjugate of Mic19. Next, we analyzed the influence of Erv1, a partner of Mia40, on the redox state of Mic19. Like the Mia40 mutants, the Erv1 conditional mutants also exhibited decreased levels of $Mic19_{con}$ (Fig. 6B). To determine whether the conjugate may consist of Mic19 that is directly and stably bound to Mia40, we performed an affinity purification assay of $Mia40_{His}$ from isolated mitochondria in wild-type strains or in a *mic19*Δ strain background. We analyzed elution fractions under reducing conditions. We observed the Mia40 partner protein Erv1 in the elution fraction, but no interaction with Mic19 was detected (Fig. 6C, left). Also, control proteins (Ccp1, Qcr8, and Cox12) were not copurified with $Mia40_{His}$. To confirm the lack of a stable interaction between Mic19 and Mia40, we analyzed the elution fraction under nonreducing conditions. If Mia40 and Mic19 directly interact with each other, then we would observe the specific band in the case of wild-type mitochondria but not in the mitochondria from the *mic19*Δ strain. However, we did not see any specific interaction in the $Mia40_{His}$ eluate, which would be absent in the *mic19*Δ deletion strain (Fig. 6C, right). Using the same approach, we analyzed the affinity purification of $Erv1_{FLAG}$ from cellular protein extracts. Mia40 was found in the eluate, in contrast to Mic19 and the control proteins (Aco1, Cyc3, Ccp1, and Cox12) (Fig. 6D, left). Like Mia40, Erv1 did not present any direct covalent interaction with Mic19 (Fig. 6D, right). These data demonstrate the functional role of the MIA pathway in the formation of the intermolecular Mic19 conjugate; however, neither Mia40 nor Erv1 was found to be a partner in the conjugate. $Mic19_{ox}$, which contains an intramolecular disulfide bond, did not depend on MIA.

The MICOS complex contains oxidized Mic19. Mic19 is the peripheral component of the MICOS complex. We sought to determine the role of other MICOS components in the biogenesis of Mic19. We first analyzed the steady-state levels of proteins from mitochondria that were isolated from all six MICOS deletion mutants (Fig. 7A). Deletion of the MICOS components was confirmed by immunodetection with specific antibodies. As previ-

Downloaded from http://mcb.asm.org/ on January 18, 2016 by NIEDERSAECHSISCHE STAATS- UND UNIVERSITAETSBIBLIOTHEK GOETTINGEN

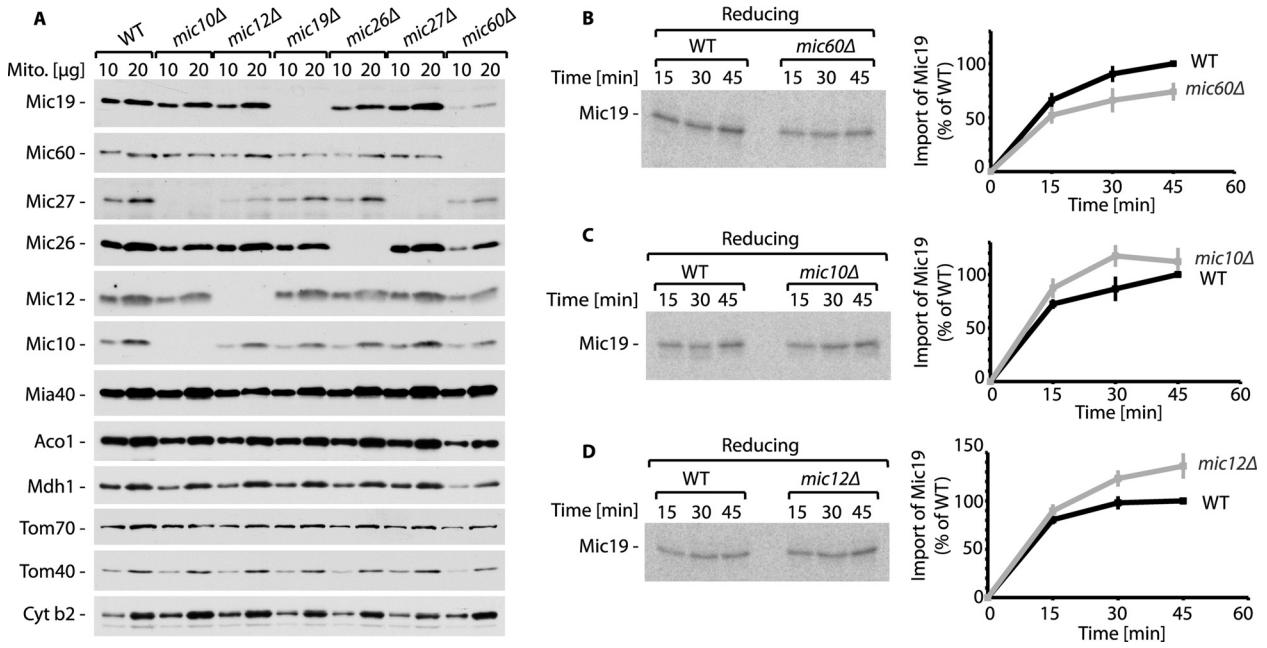

FIG 7 Mic60 is required for Mic19 biogenesis. (A) The protein levels in mitochondria isolated from the indicated yeast strains grown at 19°C are shown. The samples were analyzed by reducing SDS-PAGE followed by Western blotting. (B to D) Radiolabeled [^{35}S]Mic19 precursor protein was imported into mitochondria isolated from yeast grown at 19°C. Samples were analyzed by reducing SDS-PAGE and autoradiography. Quantifications of import efficiency are shown on the right. The level of import into wild-type mitochondria after 45 min was set equal to 100%. The means from three independent experiments are shown. Error bars indicate standard errors of the means. WT, wild type.

ously shown (4–6, 16), Mic19 levels were strongly downregulated in mitochondria from the *mic60*Δ mutant (Fig. 7A). The levels of Mic19 remained unchanged in the other MICOS deletion mutants (i.e., mutants with Mic10, Mic12, Mic26, and Mic27 deletions).

Next, we performed an *in organello* import assay and observed that the import of radiolabeled Mic19 was decreased in the *mic60*Δ mutant (Fig. 7B) but not in the *mic10*Δ or *mic12*Δ mutant (Fig. 7C and D). These data indicate that of all the MICOS components, only Mic60 plays a role in the import and biogenesis of Mic19. Mic60 is one of the key components of the MICOS complex, and the deletion of Mic60 results in disruption of the complex (4–6). This could explain the decrease in the abundance and import efficiency of Mic19 observed in mitochondria that lack Mic60. However, the depletion of Mic10, another key component of the MICOS complex that is crucial for its integrity (4–7), had no negative effect on Mic19 levels or import (Fig. 7A and C). Thus, the decrease in Mic19 abundance was not attributable to overall destabilization of the MICOS complex but was specific to Mic60 depletion. Interestingly, the import of radiolabeled Mic19 into mitochondria that were isolated from the *mic10*Δ or *mic12*Δ strain was even more efficient than that into mitochondria that were isolated from the wild type (Fig. 7C and D). The MICOS complex was previously shown to form subcomplexes with different protein compositions (5, 15, 16, 56). In the absence of one of the MICOS components, the equilibrium between components can be disturbed. Such situations may result in an excess of the Mic60-containing subcomplex, thus promoting the more efficient import of Mic19. These results indicate that the mitochondrial import of Mic19 depends on Mic60 and not on other MICOS components.

We analyzed whether MICOS components are involved in Mic19 conjugate formation. Under nonreducing conditions, Mic19 was found in an oxidized state ($Mic19_{ox}$) in mitochondria that were isolated from yeast with MICOS component deletions (i.e., *mic10*Δ, *mic12*Δ, *mic26*Δ, *mic27*Δ, and *mic60*Δ strains), albeit the amount was highly decreased in the case of the *mic60*Δ strain (Fig. 8A, lanes 1 to 7). The Mic19 conjugate ($Mic19_{con}$) was detected in mitochondria from all MICOS deletion mutants (Fig. 8A, lanes 8 to 14), demonstrating that none of the MICOS components are a direct partner in the conjugate. The oxidized form of Mic19 was diminished in mitochondria that lacked Mic60 (Fig. 8A, lanes 1 to 14). This observation shows that $Mic19_{con}$ is largely independent of the MICOS complex, in contrast to $Mix19_{ox}$.

We investigated which redox form of Mic19 is assembled into the MICOS complex by an affinity purification assay of $Mic60_{ProtA}$. We subjected the isolated mitochondria to mild reducing conditions (DTT at 20°C) before solubilizing the membranes and subsequently performing affinity purification. We observed $Mic19_{ox}$ together with $Mic60_{ProtA}$ in the eluate (Fig. 8B, lane 11). Through mild reduction, we reduced and released a pool of Mic19 from the conjugate ($Mic19_{con}$) and found that it did not bind to the MICOS complex (Fig. 8B, lane 12). These data show that the MICOS complex contains $Mix19_{ox}$.

Oxidation of Mic19 is important for MICOS stability. We analyzed whether oxidation is crucial for Mic19 assembly into the MICOS complex (Fig. 9A). We used variants of Mic19 lacking cysteine residues, which are unable to form a disulfide bond. We transformed $Mic60_{ProtA}$ *mic19*Δ yeast cells with plasmids with wild-type Mic19, single Mic19 cysteine mutants (Mic19-C146S and Mic19-C157S), a double Mic19 cysteine mutant (Mic19-C146,157S), or an empty vector as a control. In this experimental setup, we aimed to determine the ability of the Mic19 variants to

Downloaded from http://mcb.asm.org/ on January 18, 2016 by NIEDERSAECHSISCHE STAATS- UND UNIVERSITAETSBIBLIOTHEK GOETTINGEN

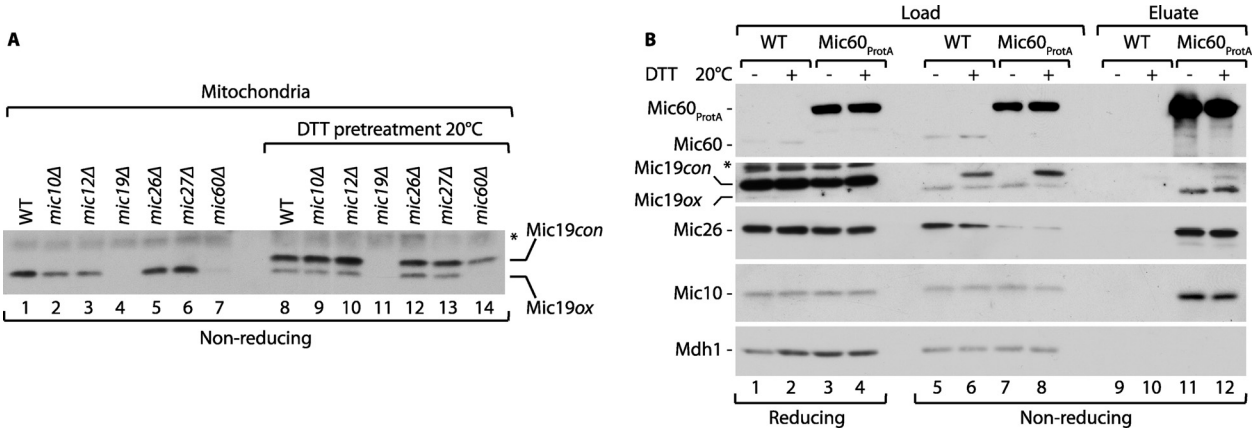

FIG 8 Mic19 assembled into the MICOS complex contains an intramolecular disulfide bond. (A) Mitochondria isolated from MICOS complex deletion mutants were incubated with IA to block the free sulfhydryl groups of cysteine residues. Where indicated, pretreatment under mild reducing conditions (DTT, 20°C) was performed. Samples were analyzed by nonreducing SDS-PAGE followed by Western blotting. ox, oxidized; con, conjugate. (B) Affinity purification of $Mic60_{ProtA}$ from isolated mitochondria. Where indicated, mitochondria were pretreated under mild reducing conditions (DTT, 20°C). Samples were analyzed by reducing and nonreducing SDS-PAGE followed by Western blotting. Load, 2%; eluate, 100%; asterisk, an unspecific signal; WT, wild type.

associate with the MICOS via the affinity purification of $Mic60_{ProtA}$ (Fig. 9A). Although none of the three cysteine mutants was oxidized, they were still able to interact with Mic60. Interestingly, we observed various behaviors of different Mic19 cysteine mutants. The Mic19-C146S variant interacted with Mic60 as efficiently as the Mic19 wild type (Fig. 9A and B). Mic19-C146,157S behaved in a variable way, and Mic19-C157S bound to Mic60 less efficiently (Fig. 9A and B). We concluded that the status of cysteine residues was not crucial for the assembly of Mic19 into the MICOS complex.

The lack of Mic19 was previously shown to cause destabilization of the MICOS complex (6). We further hypothesized that the disulfide bond of Mic19 plays a role in the stability of the MICOS complex. To test this hypothesis, we analyzed the association of other MICOS components with $Mic60_{ProtA}$ in the presence of Mic19 variants lacking cysteine residues. As expected, in the absence of Mic19, other MICOS proteins (Mic10, Mic12, and Mic26) interacted more weakly with Mic60 than the wild type (Fig. 9A and C). In mitochondria from yeast that expressed Mic19 cysteine mutants, the interaction pattern resembled that which occurred under the deletion condition (Fig. 9A and C), and the interactions between Mic60 and Mic10, Mic12, and Mic26 were remarkably decreased (Fig. 9C). Interestingly, MICOS destabilization was also observed in the case of Mic19-C146S, which was properly integrated into the MICOS complex (Fig. 9B). Thus, we concluded that the oxidation of Mic19 is required for the full stability of the MICOS complex.

The deletion of Mic19 results in a partial loss of crista junctions and, thus, in an altered (stacked or onion-like) mitochondrial IM morphology (4–6, 12), which could be rescued by expressing the Mic19 wild type from a plasmid (Fig. 9D and E). We used electron microscopy to investigate if yeast cells expressing Mic19 variants lacking cysteine residues also exhibit an altered inner membrane morphology (Fig. 9D and E). We found that yeast cells expressing Mic19 cysteine variants also displayed IM morphological changes, albeit to a lower extent than the *mic19*Δ strain. For statistical analysis, we analyzed between 250 and 850 mitochondria of each strain and assigned the IM morphology to either the normal (wild type) or an altered (stacked or onion-like) state. While ~40% of all *mic19*Δ mitochondria displayed an altered inner membrane morphology, the inner membrane morphology phenotype was less pronounced, but still observable, in the cysteine mutants. We observed an altered IM phenotype in 13%, 21%, or 20% of the mitochondria expressing Mic19-C146S, Mic19-C157S, or Mic19-C146,157S, respectively. The phenotype was more severe in cells expressing Mic19-C157S or Mic19-C146,157S than in cells expressing Mic19-C146S, although all three mutant proteins lacked the disulfide bridge. As shown above, Mic19 mutants lacking a cysteine residue in position 157 were less able to assemble into the MICOS complex (Fig. 9A and B). Therefore, the more severely altered phenotypes of Mic19-C157S and Mic19-C146,157S may be due to the additive effect of the absence of a disulfide bridge and the reduced ability to assemble into the MICOS complex. Together, the analysis of the three Mic19 mutants showed that the oxidation of Mic19 promotes the maintenance of the proper architecture of the IM by stabilizing the MICOS complex.

DISCUSSION

The MICOS complex regulates the morphology of mitochondrial IM (4–7). A vigorous branch of research has been focused on investigating the way in which the MICOS complex is organized and the specific roles that MICOS components play in the complex. On the basis of the results of studies performed on *S. cerevisiae*, Mic60 and Mic10 are considered key players in the MICOS complex, as their depletion leads to the most dramatically altered crista phenotype. Interestingly, various subcomplexes that are centered on Mic60 and Mic10 have recently been reported. The membrane-bending property of Mic10 oligomers might be critical for understanding the function of the Mic10-containing subcomplex (56, 57). Mic19 is directly linked to Mic60, forming a subcomplex that can be separated from Mic10-based subcomplexes (5, 15, 56, 58). An intriguing concept was recently proposed. According to that concept, the Mic10- and Mic60-containing subcomplexes of the MICOS are joined together by Mic19, which acts as a connector to form a functionally important entity, the MICOS holocomplex (58). These recent data suggest a unique role for Mic19 as the only component of the MICOS complex that is not embedded in the membrane.

Downloaded from http://mcb.asm.org/ on January 18, 2016 by NIEDERSAECHSISCHE STAATS- UND UNIVERSITAETSBIBLIOTHEK GOETTINGEN

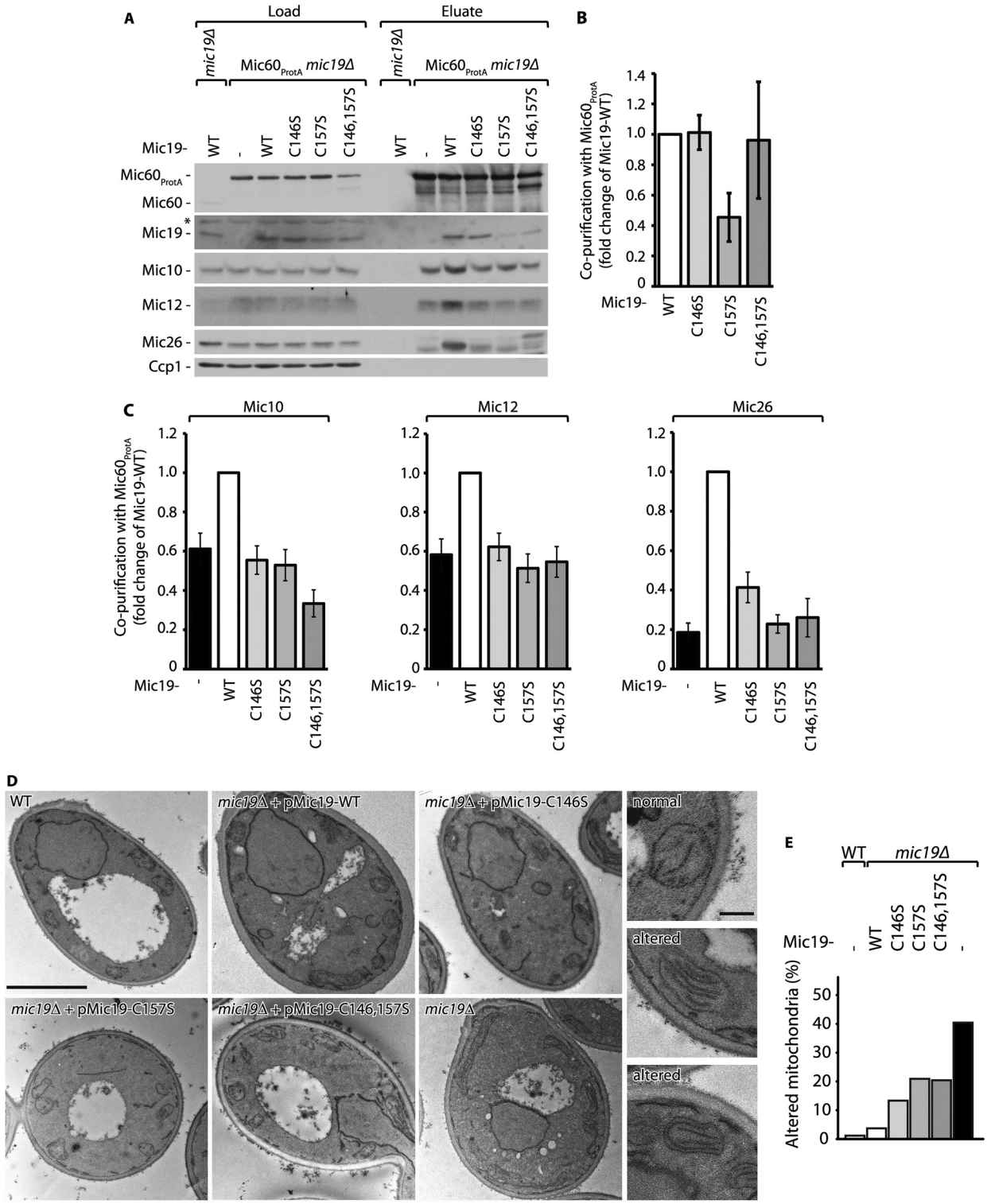

FIG 9 The integrity of MICOS depends on Mic19 oxidation. (A) Affinity purification of $Mic60_{ProtA}$ from mitochondria isolated from yeast strains with a Mic19 protein deletion or yeast strains carrying the wild-type Mic19 protein or a mutant Mic19 protein. Samples were analyzed by reducing SDS-PAGE and Western blotting. Load, 2%; eluate, 100%; asterisk, an unspecific signal. (B) Quantification of copurification of wild-type Mic19 and mutants with $Mic60_{ProtA}$. The amount of wild-type Mic19 copurified with $Mic60_{ProtA}$ was set equal to 1. The bar diagram shows mean and SEM values. The SEMs from six independent experiments are shown. (C) Quantification of copurification of Mic10, Mic12, and Mic26 with $Mic60_{ProtA}$ in the presence of wild-type Mic19 or Mic19 mutants or in the *mic19*Δ strain as a control. The amount of copurified proteins in the presence of wild-type Mic19 was set equal to 1. The bar diagram shows mean and SEM values. SEMs from six (Mic10 and Mic12) or five (Mic26) independent experiments are shown. WT, wild type. (D) Representative EM images of the various yeast strains, as indicated, and magnifications (right) of mitochondria with inner membrane morphologies referred to as normal or altered. Bars, 2 μm (overview images) and 300 nm (magnifications). (E) Quantitative analysis of the mitochondrial inner membrane morphology observed in the EM sections. For each strain, 250 to 850 mitochondria were evaluated.

Downloaded from http://mcb.asm.org/ on January 18, 2016 by NIEDERSAECHSISCHE STAATS- UND UNIVERSITAETSBIBLIOTHEK GOETTINGEN

In the present study, we focused on a systematic analysis of the biogenesis and maturation of the Mic19 protein. We directly assessed the redox status of the human MIC19 protein and found that 4 cysteine residues of the CHCH domain of MIC19 form two disulfide bonds. Moreover, we showed that the mitochondrial localization of MIC19 depends on MIA40. These findings are consistent with the observation that MIC19 interacts with MIA40 (41). In contrast to human MIC19, yeast Mic19 does not possess a standard twin Cys-X_9-Cys motif but, rather, has a simplified Cys-X_{10}-Cys motif. Our analysis of yeast Mic19 revealed that its Cys-X_{10}-Cys motif forms a disulfide bond that corresponds to the inner disulfide bond of human MIC19 between Cys193 and Cys204.

Interestingly, we observed that Mic19, apart from an oxidized monomer, forms an additional stable redox-regulated conjugate. Formation of this conjugate strictly depends on the MIA pathway, but we observed no Mic19 intermediate that is associated with Mia40 or Erv1. This raises the possibility that either a protein partner engaged with Mic19 in the conjugate is a MIA substrate or the biogenesis of the Mic19 conjugate requires MIA. Additionally, all MICOS components were excluded as potential conjugate constituents, and the MICOS preferentially interacted with the Mic19 monomer with an intramolecular disulfide bond. Therefore, Mic19 exists in mitochondria in two pools: MICOS-bound $Mic19_{ox}$ and $Mic19_{con}$ that is independent of the MICOS complex. It would be of great interest in the future to identify the Mic19 partner in the conjugate and elucidate the role of this interaction. The presence of various forms of Mic19 raises the intriguing possibility of redox-driven regulation of the MICOS complex.

Reduced cysteine mutants of human MIC19 were previously shown to be unable to efficiently bind to MIC60 (41). In the present study, in *S. cerevisiae* we found that the interaction between Mic60 and oxidized Mic19 is indeed preferable. However, Mic60 efficiently binds to the reduced Mic19-C146S mutant, suggesting that oxidation is not essential for the interaction with Mic60. As previously reported, the deletion of Mic19 results in destabilization of the MICOS complex (4–6). Interestingly, Mic19-C146S, which lacks a disulfide bond, despite its efficient binding to Mic60, caused destabilization of the MICOS complex (i.e., decreased interactions between Mic60 and Mic10, Mic12, and Mic26). This effect differs from the recently reported effect that is exerted by the absence of Cox17, a copper chaperone for cytochrome *c* oxidase with an additional role as an assembly/stabilization factor for the MICOS complex. In the absence of Cox17, Mic60 less efficiently interacts with several MICOS components, including Mic19 (59). MICOS destabilization through reduced Mic19 resulted in changes in IM morphology that resembled the effect of Mic19 deletion, albeit to a lesser extent. Interestingly, the Mic10, Mic12, and Mic26 components, which do not bind to Mic60 in the presence of Mic19-C146S, were consistently shown to constitute a Mic60-independent MICOS subcomplex (15, 56, 58). Thus, a tempting proposition is that a disulfide bond in Mic19 promotes the structural role of Mic19 as a connector between two MICOS subcomplexes. The pool of intermolecularly oxidized Mic19 ($Mic19_{con}$) may regulate the amount of Mic19 that is necessary to serve a connector function for the MICOS complex.

In summary, we have described the biogenesis of Mic19 and its dependence on the MIA pathway. We showed that Mic19 undergoes oxidation in mitochondria, which, although not essential for its integration into the MICOS complex, is important for formation of the MICOS holocomplex and the effective regulation of the membrane architecture.

ACKNOWLEDGMENTS

We thank Peter Rehling, Markus Deckers, and Sven Dennerlein for discussion and expertise.

Research in the A.C. laboratory is supported by the National Science Centre (NCN; grants 2011/02/B/NZ2/01402 and 2013/11/B/NZ3/00974) and Ministerial Ideas Plus program 000263. S.J. acknowledges support by the Cluster of Excellence and DFG Research Center Nanoscale Microscopy and Molecular Physiology of the Brain. P.S. was supported by NCN grant 2011/03/N/NZ3/01614. K.M. was supported by NCN grant 2012/05/B/NZ3/00781.

We declare that we have no conflict of interest.

REFERENCES

1. **Frey TG, Mannella CA.** 2000. The internal structure of mitochondria. Trends Biochem Sci **25:**319–324. http://dx.doi.org/10.1016/S0968-0004(00)01609-1.
2. **Zick M, Rabl R, Reichert AS.** 2009. Cristae formation-linking ultrastructure and function of mitochondria. Biochim Biophys Acta **1793:**5–19. http://dx.doi.org/10.1016/j.bbamcr.2008.06.013.
3. **Rabl R, Soubannier V, Scholz R, Vogel F, Mendl N, Vasiljev-Neumeyer A, Körner C, Jagasia R, Keil T, Baumeister W, Cyrklaff M, Neupert W, Reichert AS.** 2009. Formation of cristae and crista junctions in mitochondria depends on antagonism between Fcj1 and Su e/g. J Cell Biol **185:**1047–1063. http://dx.doi.org/10.1083/jcb.200811099.
4. **Harner M, Körner C, Walther D, Mokranjac D, Kaesmacher J, Welsch U, Griffith J, Mann M, Reggiori F, Neupert W.** 2011. The mitochondrial contact site complex, a determinant of mitochondrial architecture. EMBO J **30:**4356–4370. http://dx.doi.org/10.1038/emboj.2011.379.
5. **Hoppins S, Collins SR, Cassidy-Stone A, Hummel E, Devay RM, Lackner LL, Westermann B, Schuldiner M, Weissman JS, Nunnari J.** 2011. A mitochondrial-focused genetic interaction map reveals a scaffold-like complex required for inner membrane organization in mitochondria. J Cell Biol **195:**323–340. http://dx.doi.org/10.1083/jcb.201107053.
6. **von der Malsburg K, Müller JM, Bohnert M, Oeljeklaus S, Kwiatkowska P, Becker T, Loniewska-Lwowska A, Wiese S, Rao S, Milenkovic D, Hutu DP, Zerbes RM, Schulze-Specking A, Meyer HE, Martinou JC, Rospert S, Rehling P, Meisinger C, Veenhuis M, Warscheid B, van der Klei IJ, Pfanner N, Chacinska A, van der Laan M.** 2011. Dual role of mitofilin in mitochondrial membrane organization and protein biogenesis. Dev Cell **21:**694–707. http://dx.doi.org/10.1016/j.devcel.2011.08.026.
7. **Alkhaja AK, Jans DC, Nikolov M, Vukotic M, Lytovchenko O, Ludewig F, Schliebs W, Riedel D, Urlaub H, Jakobs S, Deckers M.** 2012. MINOS1 is a conserved component of mitofilin complexes and required for mitochondrial function and cristae organization. Mol Biol Cell **23:**247–257. http://dx.doi.org/10.1091/mbc.E11-09-0774.
8. **Jans DC, Wurm CA, Riedel D, Wenzel D, Stagge F, Deckers M, Rehling P, Jakobs S.** 2013. STED super-resolution microscopy reveals an array of MINOS clusters along human mitochondria. Proc Natl Acad Sci U S A **110:**8936–8941. http://dx.doi.org/10.1073/pnas.1301820110.
9. **Pfanner N, van der Laan M, Amati P, Capaldi RA, Caudy AA, Chacinska A, Darshi M, Deckers M, Hoppins S, Icho T, Jakobs S, Ji J, Kozjak-Pavlovic V, Meisinger C, Odgren PR, Park SK, Rehling P, Reichert AS, Sheikh MS, Taylor SS, Tsuchida N, van der Bliek AM, van der Klei IJ, Weissman JS, Westermann B, Zha J, Neupert W, Nunnari J.** 2014. Uniform nomenclature for the mitochondrial contact site and cristae organizing system. J Cell Biol **204:**1083–1086. http://dx.doi.org/10.1083/jcb.201401006.
10. **John GB, Shang Y, Li L, Renken C, Mannella CA, Selker JM, Rangell L, Bennett MJ, Zha J.** 2005. The mitochondrial inner membrane protein mitofilin controls cristae morphology. Mol Biol Cell **16:**1543–1554. http://dx.doi.org/10.1091/mbc.E04-08-0697.
11. **Xie J, Marusich MF, Souda P, Whitelegge J, Capaldi RA.** 2007. The mitochondrial inner membrane protein mitofilin exists as a complex with SAM50, metaxins 1 and 2, coiled-coil-helix coiled-coil-helix domain-containing protein 3 and 6 and DnaJC11. FEBS Lett **581:**3545–3549. http://dx.doi.org/10.1016/j.febslet.2007.06.052.
12. **Darshi M, Mendiola VL, Mackey MR, Murphy AN, Koller A, Perkins**

Downloaded from http://mcb.asm.org/ on January 18, 2016 by NIEDERSAECHSISCHE STAATS- UND UNIVERSITAETSBIBLIOTHEK GOETTINGEN

GA, Ellisman MH, Taylor SS. 2011. ChChd3, an inner mitochondrial membrane protein, is essential for maintaining crista integrity and mitochondrial function. J Biol Chem **286:**2918–2932. http://dx.doi.org/10.1074/jbc.M110.171975.

13. **An J, Shi J, He Q, Lui K, Liu Y, Huang Y, Sheikh MS.** 2012. CHCM1/CHCHD6, novel mitochondrial protein linked to regulation of mitofilin and mitochondrial cristae morphology. J Biol Chem **287:**7411–7426. http://dx.doi.org/10.1074/jbc.M111.277103.
14. **Weber TA, Koob S, Heide H, Wittig I, Head B, van der Bliek A, Brandt U, Mittelbronn M, Reichert AS.** 2013. APOOL is a cardiolipin-binding constituent of the Mitofilin/MINOS protein complex determining cristae morphology in mammalian mitochondria. PLoS One **8:**e63683. http://dx.doi.org/10.1371/journal.pone.0063683.
15. **Guarani V, McNeill EM, Paulo JA, Huttlin EL, Fröhlich F, Gygi SP, Van Vactor D, Harper JW.** 2015. QIL1 is a novel mitochondrial protein required for MICOS complex stability and cristae morphology. eLife **4:**e06265. http://dx.doi.org/10.7554/eLife.06265.
16. **Ott C, Dorsch E, Fraunholz M, Straub S, Kozjak-Pavlovic V.** 2015. Detailed analysis of the human mitochondrial contact site complex indicate a hierarchy of subunits. PLoS One **10:**e0120213. http://dx.doi.org/10.1371/journal.pone.0120213.
17. **Mun JY, Lee TH, Kim JH, Yoo BH, Bahk YY, Koo HS, Han SS.** 2010. Caenorhabditis elegans mitofilin homologs control the morphology of mitochondrial cristae and influence reproduction and physiology. J Cell Physiol **224:**748–756. http://dx.doi.org/10.1002/jcp.22177.
18. **Head BP, Zulaika M, Ryazantsev S, van der Bliek AM.** 2011. A novel mitochondrial outer membrane protein, MOMA-1, that affects cristae morphology in Caenorhabditis elegans. Mol Biol Cell **22:**831–841. http://dx.doi.org/10.1091/mbc.E10-07-0600.
19. **Bohnert M, Wenz LS, Zerbes RM, Horvath SE, Stroud DA, von der Malsburg K, Müller JM, Oeljeklaus S, Perschil I, Warscheid B, Chacinska A, Veenhuis M, van der Klei IJ, Daum G, Wiedemann N, Becker T, Pfanner N, van der Laan M.** 2012. Role of mitochondrial inner membrane organizing system in protein biogenesis of the mitochondrial outer membrane. Mol Biol Cell **23:**3948–3956. http://dx.doi.org/10.1091/mbc.E12-04-0295.
20. **Körner C, Barrera M, Dukanovic J, Eydt K, Harner M, Rabl R, Vogel F, Rapaport D, Neupert W, Reichert AS.** 2012. The C-terminal domain of Fcj1 is required for formation of crista junctions and interacts with the TOB/SAM complex in mitochondria. Mol Biol Cell **23:**2143–2155. http://dx.doi.org/10.1091/mbc.E11-10-0831.
21. **Ott C, Ross K, Straub S, Thiede B, Götz M, Goosmann C, Krischke M, Mueller MJ, Krohne G, Rudel T, Kozjak-Pavlovic V.** 2012. Sam50 functions in mitochondrial intermembrane space bridging and biogenesis of respiratory complexes. Mol Cell Biol **32:**1173–1188. http://dx.doi.org/10.1128/MCB.06388-11.
22. **van der Laan M, Bohnert M, Wiedemann N, Pfanner N.** 2012. Role of MINOS in mitochondrial membrane architecture and biogenesis. Trends Cell Biol **22:**185–192. http://dx.doi.org/10.1016/j.tcb.2012.01.004.
23. **Zerbes RM, Bohnert M, Stroud DA, von der Malsburg K, Kram A, Oeljeklaus S, Warscheid B, Becker T, Wiedemann N, Veenhuis M, van der Klei IJ, Pfanner N, van der Laan M.** 2012. Role of MINOS in mitochondrial membrane architecture: cristae morphology and outer membrane interactions differentially depend on mitofilin domains. J Mol Biol **422:**183–191. http://dx.doi.org/10.1016/j.jmb.2012.05.004.
24. **Neupert W, Herrmann JM.** 2007. Translocation of proteins into mitochondria. Annu Rev Biochem **76:**723–749. http://dx.doi.org/10.1146/annurev.biochem.76.052705.163409.
25. **Chacinska A, Koehler CM, Milenkovic D, Lithgow T, Pfanner N.** 2009. Importing mitochondrial proteins: machineries and mechanisms. Cell **138:**628–644. http://dx.doi.org/10.1016/j.cell.2009.08.005.
26. **Schmidt O, Pfanner N, Meisinger C.** 2010. Mitochondrial protein import: from proteomics to functional mechanisms. Nat Rev Mol Cell Biol **11:**655–667. http://dx.doi.org/10.1038/nrm2959.
27. **Sokol AM, Sztolsztener ME, Wasilewski M, Heinz E, Chacinska A.** 2014. Mitochondrial protein translocases for survival and wellbeing. FEBS Lett **588:**2484–2495. http://dx.doi.org/10.1016/j.febslet.2014.05.028.
28. **Herrmann JM, Riemer J.** 2010. The intermembrane space of mitochondria. Antioxid Redox Signal **13:**1341–1358. http://dx.doi.org/10.1089/ars.2009.3063.
29. **Stojanovski D, Bragoszewski P, Chacinska A.** 2012. The MIA pathway: a tight bond between protein transport and oxidative folding in mitochondria. Biochim Biophys Acta **1823:**1142–1150. http://dx.doi.org/10.1016/j.bbamcr.2012.04.014.
30. **Mesecke N, Terziyska N, Kozany C, Baumann F, Neupert W, Hell K, Herrmann JM.** 2005. A disulfide relay system in the intermembrane space of mitochondria that mediates protein import. Cell **121:**1059–1069. http://dx.doi.org/10.1016/j.cell.2005.04.011.
31. **Banci L, Bertini I, Cefaro C, Ciofi-Baffoni S, Gallo A, Martinelli M, Sideris DP, Katrakili N, Tokatlidis K.** 2009. MIA40 is an oxidoreductase that catalyzes oxidative protein folding in mitochondria. Nat Struct Mol Biol **16:**198–206. http://dx.doi.org/10.1038/nsmb.1553.
32. **Sideris DP, Tokatlidis K.** 2010. Oxidative protein folding in the mitochondrial intermembrane space. Antioxid Redox Signal **13:**1189–1204. http://dx.doi.org/10.1089/ars.2010.3157.
33. **Herrmann JM, Riemer J.** 2012. Mitochondrial disulfide relay: redox-regulated protein import into the intermembrane space. J Biol Chem **287:**4426–4433. http://dx.doi.org/10.1074/jbc.R111.270678.
34. **Chacinska A, Pfannschmidt S, Wiedemann N, Kozjak V, Sanjuán Szklarz LK, Schulze-Specking A, Truscott KN, Guiard B, Meisinger C, Pfanner N.** 2004. Essential role of Mia40 in import and assembly of mitochondrial intermembrane space proteins. EMBO J **23:**3735–3746. http://dx.doi.org/10.1038/sj.emboj.7600389.
35. **Koehler CM.** 2004. The small Tim proteins and the twin Cx3C motif. Trends Biochem Sci **29:**1–4. http://dx.doi.org/10.1016/j.tibs.2003.11.003.
36. **Gabriel K, Milenkovic D, Chacinska A, Müller J, Guiard B, Pfanner N, Meisinger C.** 2007. Novel mitochondrial intermembrane space proteins as substrates of the MIA import pathway. J Mol Biol **365:**612–620. http://dx.doi.org/10.1016/j.jmb.2006.10.038.
37. **Longen S, Bien M, Bihlmaier K, Kloeppel C, Kauff F, Hammermeister M, Westermann B, Herrmann JM, Riemer J.** 2009. Systematic analysis of the twin cx(9)c protein family. J Mol Biol **393:**356–368. http://dx.doi.org/10.1016/j.jmb.2009.08.041.
38. **Stojanovski D, Milenkovic D, Müller JM, Gabriel K, Schulze-Specking A, Baker MJ, Ryan MT, Guiard B, Pfanner N, Chacinska A.** 2008. Mitochondrial protein import: precursor oxidation in a ternary complex with disulfide carrier and sulfhydryl oxidase. J Cell Biol **183:**195–202. http://dx.doi.org/10.1083/jcb.200804095.
39. **Banci L, Bertini I, Calderone V, Cefaro C, Ciofi-Baffoni S, Gallo A, Kallergi E, Lionaki E, Pozidis C, Tokatlidis K.** 2011. Molecular recognition and substrate mimicry drive the electron-transfer process between MIA40 and ALR. Proc Natl Acad Sci U S A **108:**4811–4816. http://dx.doi.org/10.1073/pnas.1014542108.
40. **Böttinger L, Gornicka A, Czerwik T, Bragoszewski P, Loniewska-Lwowska A, Schulze-Specking A, Truscott KN, Guiard B, Milenkovic D, Chacinska A.** 2012. In vivo evidence for cooperation of Mia40 and Erv1 in the oxidation of mitochondrial proteins. Mol Biol Cell **23:**3957–3969. http://dx.doi.org/10.1091/mbc.E12-05-0358.
41. **Darshi M, Trinh KN, Murphy AN, Taylor SS.** 2012. Targeting and import mechanism of coiled-coil helix coiled-coil helix domain-containing protein 3 (ChChd3) into the mitochondrial intermembrane space. J Biol Chem **287:**39480–39491. http://dx.doi.org/10.1074/jbc.M112.387696.
42. **Hofmann S, Rothbauer U, Mühlenbein N, Baiker K, Hell K, Bauer MF.** 2005. Functional and mutational characterization of human MIA40 acting during import into the mitochondrial intermembrane space. J Mol Biol **353:**517–528. http://dx.doi.org/10.1016/j.jmb.2005.08.064.
43. **Polimeno L, Pesetti B, De Santis F, Resta L, Rossi R, De Palma A, Girardi B, Amoruso A, Francavilla A.** 2012. Decreased expression of the augmenter of liver regeneration results in increased apoptosis and oxidative damage in human-derived glioma cells. Cell Death Dis **3:**e289. http://dx.doi.org/10.1038/cddis.2012.25.
44. **Meisinger C, Pfanner N, Truscott KN.** 2006. Isolation of yeast mitochondria. Methods Mol Biol **313:**33–39. http://dx.doi.org/10.1385/1-59259-958-3:033.
45. **Yamaguchi R, Andreyev A, Murphy AN, Perkins GA, Ellisman MH, Newmeyer DD.** 2007. Mitochondria frozen with trehalose retain a number of biological functions and preserve outer membrane integrity. Cell Death Differ **14:**616–624. http://dx.doi.org/10.1038/sj.cdd.4402035.
46. **Milenkovic D, Ramming T, Müller JM, Wenz LS, Gebert N, Schulze-Specking A, Stojanovski D, Rospert S, Chacinska A.** 2009. Identification of the signal directing Tim9 and Tim10 into the intermembrane space of mitochondria. Mol Biol Cell **20:**2530–2539. http://dx.doi.org/10.1091/mbc.E08-11-1108.
47. **Wrobel L, Trojanowska A, Sztolsztener ME, Chacinska A.** 2013. Mito-

Downloaded from http://mcb.asm.org/ on January 18, 2016 by NIEDERSAECHSISCHE STAATS- UND UNIVERSITAETSBIBLIOTHEK GOETTINGEN

chondrial protein import: Mia40 facilitates Tim22 translocation into the inner membrane of mitochondria. Mol Biol Cell **24:**543–554. http://dx.doi.org/10.1091/mbc.E12-09-0649.
48. **Sherman F.** 2002. Getting started with yeast. Methods Enzymol **350:**3–41. http://dx.doi.org/10.1016/S0076-6879(02)50954-X.
49. **Erdmann R, Veenhuis M, Mertens D, Kunau WH.** 1989. Isolation of peroxisome-deficient mutants of Saccharomyces cerevisiae. Proc Natl Acad Sci U S A **86:**5419–5423. http://dx.doi.org/10.1073/pnas.86.14.5419.
50. **Weckbecker D, Longen S, Riemer J, Herrmann JM.** 2012. Atp23 biogenesis reveals a chaperone-like folding activity of Mia40 in the IMS of mitochondria. EMBO J **31:**4348–4358. http://dx.doi.org/10.1038/emboj.2012.263.
51. **Longen S, Woellhaf MW, Petrungaro C, Riemer J, Herrmann JM.** 2014. The disulfide relay of the intermembrane space oxidizes the ribosomal subunit mrp10 on its transit into the mitochondrial matrix. Dev Cell **28:**30–42. http://dx.doi.org/10.1016/j.devcel.2013.11.007.
52. **Bragoszewski P, Wasilewski M, Sakowska P, Gornicka A, Böttinger L, Qiu J, Wiedemann N, Chacinska A.** 2015. Retro-translocation of mitochondrial intermembrane space proteins. Proc Natl Acad Sci U S A **112:**7713–7718. http://dx.doi.org/10.1073/pnas.1504615112.
53. **Qiu J, Wenz LS, Zerbes RM, Oeljeklaus S, Bohnert M, Stroud DA, Wirth C, Ellenrieder L, Thornton N, Kutik S, Wiese S, Schulze-Specking A, Zufall N, Chacinska A, Guiard B, Hunte C, Warscheid B, van der Laan M, Pfanner N, Wiedemann N, Becker T.** 2013. Coupling of mitochondrial import and export translocases by receptor-mediated supercomplex formation. Cell **154:**596–608. http://dx.doi.org/10.1016/j.cell.2013.06.033.
54. **Chacinska A, Lind M, Frazier AE, Dudek J, Meisinger C, Geissler A, Sickmann A, Meyer HE, Truscott KN, Guiard B, Pfanner N, Rehling P.** 2005. Mitochondrial presequence translocase: switching between TOM tethering and motor recruitment involves Tim21 and Tim17. Cell **120:**817–829. http://dx.doi.org/10.1016/j.cell.2005.01.011.
55. **Sztolsztener ME, Brewinska A, Guiard B, Chacinska A.** 2013. Disulfide bond formation: sulfhydryl oxidase ALR controls mitochondrial biogenesis of human MIA40. Traffic **14:**309–320. http://dx.doi.org/10.1111/tra.12030.
56. **Bohnert M, Zerbes RM, Davies KM, Mühleip AW, Rampelt H, Horvath SE, Boenke T, Kram A, Perschil I, Veenhuis M, Kühlbrandt W, van der Klei IJ, Pfanner N, van der Laan M.** 2015. Central role of mic10 in the mitochondrial contact site and cristae organizing system. Cell Metab **21:**747–755. http://dx.doi.org/10.1016/j.cmet.2015.04.007.
57. **Barbot M, Jans DC, Schulz C, Denkert N, Kroppen B, Hoppert M, Jakobs S, Meinecke M.** 2015. Mic10 oligomerizes to bend mitochondrial inner membranes at cristae junctions. Cell Metab **21:**756–763. http://dx.doi.org/10.1016/j.cmet.2015.04.006.
58. **Friedman JR, Mourier A, Yamada J, McCaffery JM, Nunnari J.** 2015. MICOS coordinates with respiratory complexes and lipids to establish mitochondrial inner membrane architecture. eLife **4:**e07739. http://dx.doi.org/10.7554/eLife.07739.
59. **Chojnacka M, Gornicka A, Oeljeklaus S, Warscheid B, Chacinska A.** 2015. Cox17 protein is an auxiliary factor involved in the control of the mitochondrial contact site and cristae organizing system. J Biol Chem **290:**15304–15312. http://dx.doi.org/10.1074/jbc.M115.645069.
60. **Sikorski RS, Hieter P.** 1989. A system of shuttle vectors and yeast host strains designed for efficient manipulation of DNA in Saccharomyces cerevisiae. Genetics **122:**19–27.

Downloaded from http://mcb.asm.org/ on January 18, 2016 by NIEDERSAECHSISCHE STAATS- UND UNIVERSITAETSBIBLIOTHEK GOETTINGEN